Site Effects Assessment Using Ambient Excitations

SESAME

European Commission – Research General Directorate
Project No. EVG1-CT-2000-00026 SESAME

Final report

WP08

Nature of noise wavefield

Deliverable D13.08

July 2004

List of Contents

List of Contributors

Sylvette Bonnefoy-Claudet   LGIT, Grenoble, France
Cécile Cornou   ETHZ, Zurich, Switzerland
Pierre-Yves Bard   LGIT, Grenoble, France
Fabrice Cotton   LGIT, Grenoble, France

Project coordinator: Pierre-Yves Bard   LGIT, Grenoble, France
Task C Leader: Pierre-Yves Bard   LGIT, Grenoble, France
WP08 Leader: Pierre-Yves Bard   LGIT, Grenoble, France

Summary

In the following we report the results of the nature of noise wavefield. This work was conducted under the framework of the **SESAME Project** (Site Effects Assessment Using Ambient Excitations, EC-RGD, Project No. EVG1-CT-2000-00026 SESAME), Task C (physical background and noise simulation), Work Package 08 (WP08 – Nature of Noise Wavefield).

Introduction

The objectives of the WP08 of the SESAME project are to clarify our knowledge about the physical nature of noise wavefield in urban areas.

The first step of this study is devoted to update the literature survey in order to increase our knowledge on the actual consistency of the noise wavefield. Then, in a second part, in order to separate body waves and surface waves, we investigate the nature of noise wavefield through numerical simulation under well controlled simple 1D structure (one sedimentary layer over bedrock).

Chapter 1: Literature survey

1 Introduction

Since several years, seismic hazard in urbanized cities such as Quito, Mexico, San Francisco has been assumed by scientists and politics. Since part of damages is due to site effects, it is important to determine the soil response during an earthquake.

Geophysical techniques usually used to determine the soil characteristic (seismic reflexion and refraction, borehole...) are not adapted in urbanised areas. In other hand, noise techniques are a good alternative since they do not need external sources (explosive or vibrational sources), are easy to use, and are cheaper than traditional geophysical techniques.

The spectral ratio of horizontal and vertical components and array studies are the two main noise techniques used. The first one is based on the ellipticity property of Rayleigh waves to estimate the fundamental frequency and the amplification of soil. Assuming that noise is constituted by fundamental Rayleigh waves, array studies allow to determine the shear waves velocity profile of soil.

These methods are strongly linked with the nature of noise wavefield: seismic noise must be constituted by fundamental Rayleigh waves. However, until now, nobody provided clear and unanimous conclusions about the nature of noise. That is why within the framework of the SESAME project we have updated a survey of the scientific literature dealing with seismic noise, in order to establish a state of art about the knowledge of the origin and the nature of noise in determining these three ratios:
-    the ratio of body waves to surface waves;
-    the ratio of Love waves to Rayleigh waves;
-    the ratio of the fundamental Rayleigh mode to higher modes.

Before reviewing the learning from the literature about these three ratios, let start with a short description of the main historical periods in noise literature.

2 Main historical periods

Microtremors have been observed very early from the beginning of the nineteenth century. In 1872, Bertelli installed a pendulum and observed during many years that sometimes the pendulum moved continuously for hours or days. He noticed a correlation between the "microseisms" and disturbed air pressure (Gutenberg 1958). Since this date many studies about noise have been carried out. We can distinguish three predominant time periods.

Until the middle of the twentieth century, studies were more qualitative than quantitative: progress in knowledge was limited by instrumental techniques. However, some authors highlighted important characteristics of noise. Relations between microseisms, meteorological conditions and oceanic waves have been pointed out by Banerji (Banerji 1924, 1925). He observed microseisms associated with Indian monsoon

in south Asia, and suggested that they are due to Rayleigh waves set up at the bottom of the sea by the train of water waves maintained by the monsoon currents.

In 1858, Gutenberg (Gutenberg 1958) quoted a bibliography containing 600 references about microseisms. Unfortunately, the major part of these references is in foreign language (Russian, German, Italian ...) and they were published in local scientific journal. It is difficult to obtain a copy of these noise references until the 50's.

During the 50-70's, expansion of seismology and equipment technical improvement (seismometers, data logger) allowed significant advances in the understanding of noise phenomena. Several authors felt the interest to use the noise (different application), and investigated the origin and the nature of noise. Several techniques using noise have been developed. The most important are the array technique (wave time delay measurements between coupled stations). These methods are linked with the property of surface waves dispersion, and give the opportunity to obtain the shear waves velocity profile of soil. There are two main arrays techniques: the frequency-wave number analysis (F-K) (Capon, et al. 1967, Capon 1969, Lacoss, et al. 1969), and the spatial autocorrelation analysis of signal (SPAC) (Aki 1957, 1964).

To investigate the noise wavefield, others methods have been used such as particle motion (Toksöz 1964), or boreholes techniques sometimes coupled with arrays analysis (Douze 1964, Gupta 1965, Douze 1967).

The emergence of these techniques has been useful for improving our knowledge about the origin of noise (oceanic, meteorological, human ...) and the nature of noise wavefield.

Since the 80's up to now, the number of microtremor publications has increased every year. As it is not easy to reach all the publications (especially in Japanese literature), we estimate the number of microtremor publications to be about 500. Some of them are devoted to the nature of noise wavefield, but an overwhelming majority (about 95%) is dealing with the applicability of microtremor, and/or their direct applications to some specific case studies.

The most important application is seismic microzonation of cities. There are two major techniques: site to reference spectral ratios, and H/V ratio. The second method is more widely used than the first one. The H/V ratio technique has been proposed first by (Nogoshi, et al. 1971), and then strongly emphasized by Nakamura (Nakamura 1989, 2000). Since this date, many authors have published papers about microzonation done using H/V ratio (Ansary, et al. 1995, Field, et al. 1995, Gaull, et al. 1995, Theodulidis, et al. 1995, Abeki, et al. 1996, Konno 1996, Teves-Costa, et al. 1996, Wakamatsu, et al. 1996, Alfaro, et al. 1997, Fäh 1997, Abeki, et al. 1998, Bour, et al. 1998, Duval, et al. 1998, Guéguen, et al. 1998, Ishida, et al. 1998, Konno, et al. 1998, Mucciarelli 1998, Ogawa, et al. 1998, Ibs-Von Seht, et al. 1999, Al Yuncha, et al. 2000, Maruyama, et al. 2000, Tobita, et al. 2000, Alfaro, et al. 2001, Ansal, et al. 2001, Bindi, et al. 2001, Duval, et al. 2001, Duval, et al. 2001, Giampiccolo, et al. 2001, Lebrun, et al. 2001, Lombardo, et al. 2001, Delgado, et al. 2002, Huang, et al. 2002, Parolai, et al. 2002, Cara, et al. 2003, Maresca, et al. 2003, Uebayashi 2003); see (Kudo 1995, Bard 1998) for a review). Although few authors (Lermo, et al. 1993, Lachet, et al. 1994, Kudo 1995, Delgado, et al. 2000, Luzon, et al. 2001, Rodriguez, et al. 2003) attempted to find qualitative explanations about Nakamura's technique, the major part of the authors assume that the method basements are right.

An other application of noise background vibration is the use of array technique to obtain subsurface velocity profile. Such studies started in the late 50's, but improvements in computer, and instrumental techniques (3-components seismometer, numeric data), in the last 3 decades, allow quantity and quality increase of array surveys data recording (Asten, et al. 1984, Bache, et al. 1986, Tokimatsu, et al. 1992, Malagnini, et al. 1993, Arai, et al. 1996, Horike 1996, Kagawa 1996, Milana, et al. 1996, Miyakoshi, et al. 1996, Tokimatsu, et al. 1996, Friedrich, et al. 1998, Miyakoshi, et al. 1998, Maresca, et al. 1999, Scherbaum, et al. 1999, Kanno, et al. 2000, Liu, et al. 2000, Bettig, et al. 2001, Satoh, et al. 2001, Kudo, et al. 2002, Ohori, et al. 2002, Flores Estrella, et al. 2003, Scherbaum, et al. 2003).

In most of these studies the authors assume that the nature and origin of microtremor are (well) known, and do not discuss about this issue. It is usual to read in such papers that the authors assume that microtremor consist in surface waves without any more discussion about the noise parameters.

3 Origin of noise

Noise is the generic term used to denote ambient vibrations of the ground caused by sources such as tide, water waves striking the coast, turbulent wind, effects of wind on trees or buildings, industrial machinery, cars and trains, or men steps ... the list is long but not exhaustive!

It does seem uneasy to classify clearly all the noise sources. In 1958 Gutenberg established a list of the different types of sources according to frequency (Gutenberg 1958). Several years later, Asten establish the same conclusions in a noise review (Asten 1978, Asten and Henstridge 1984). A synthesis about this frequency dependency of noise sources is shown in Table 1-1. However, if we consider the nature of these sources, a suitable criterion appears: the natural or anthropic typical origin. This criterion let to distinguish between microseisms and microtremor, corresponding to natural and anthropic sources.

According to the synthesis of Gutenberg and Asten we can conclude, in first approximation, that at low frequency (below 1 Hz) sources are natural (ocean, large scale meteorological conditions); at intermediate frequency (between 1 to 5 Hz) sources are either natural (local meteorological conditions) or anthropic (urban); at higher frequency (above 1 Hz) sources are essentially anthropic.

Extensive investigations achieved by Frantti suggest a change in the noise behaviour around 1 Hz (Frantti, et al. 1962, Frantti 1963). He measured the ground particle velocity of seismic noise on 48 sites in the United States and foreign countries. These noise measurements have been performed at different geological sites (rock or sediment), at different geographical localisations (close to ocean, mountain, or city), and at different time (variability on hours and seasons). For the processing a two-minute record interval was selected which is free from any known nearby disturbances. Measurements were made with 1s Benioff and Willmore three-component seismometers, and 2s Hall-Sears geophones. Vertical component of noise particle velocities are plotted against frequency (in cps) in Figure 1-1. The consistent decrease of seismic noise up to 1 Hz (1 cps), and the flat level for higher frequencies are similar for all sites, while the absolute level exhibit large changes from site to site.

These observations point out the link between the source type (natural or anthropic) and the behaviour in the spectral domain. According to the works of Gutenberg and Asten, the limit between low frequency "natural" microseisms and higher frequency "anthropic" microtremors is around 1 Hz.

Yamanaka et al., in 1993, published interesting results about noise spectral behaviour over time (Yamanaka, et al. 1993). They performed continuous noise measurements (10 minutes every 2 hours) on the campus of the University of Southern California in Los Angeles, between 17 and 25 September 1990. This site is characterized by the existence of deep sediments. The instruments (two horizontal seismometers with a natural period 0.8s increased to 12s) are installed on underground floor of a three-story building. Figure 1-2 displays the time variant characteristics of the spectral amplitude at period of 0.3s and 6.5s (they calculated the geometric means of the two horizontal spectra). For comparison swell height observed at Begg Rock, California, is also represented. This is an oceanic buoy station located about 100 km southwest of the Los Angeles coast.

A regular and daily spectral amplitude variation showing the minimum in mid-night time and the maximum in mid-daytime can be clearly identified for the microtremors in a period of 0.3s. Moreover, the spectral amplitude on Saturdays and Sundays are smaller than over the week. These results indicate that the microtremors in a period of 0.3s are caused by cultural activities. The spectral amplitude in a period of 6.5s, however, varies differently with time. The amplitude becomes gradually larger after the 20 September. After the amplitude reaches the maximum at approximately noon on 22 September, it decreases and returns on 23 September to an amplitude similar to that before 20 September. For comparison, the swell amplitude at the Begg Rock station becomes larger on the 20 September, and reaches a maximum on 21 September. Although there is a slight delay for the maximum amplitude, we can see an agreement of the swell change with that of microseisms at long period. This similarity in the time variant characteristics indicates that the long period microseisms in the Los Angeles basin are highly related to ocean disturbances

These results emphasize the different noise behaviour in spectral domain depending on the origin of the noise, with clear physical differences between low frequency and higher frequency.

Such daily and weekly variations in spectral amplitudes of microtremors have been reported in the earlier stage of research on noise. Kanai and Tanaka (Kanai, et al. 1961) present similar results on continuous noise measurements performed in Tokyo (Japan). For two different days (13 October 1955 and 12 September 1956), they show the noise amplitude variation over 24 hours. During the daytime the maximum amplitude is contained between 0.4 and 0.5 micrometer, while during the night time this value drops to 0.1-0.2 micrometer. In the same way, they represent the average of spectral amplitude over time, and show that the

predominant period of microtremor is different according to hours (higher period during night time than daytime). Moreover, they perform noise measurements during daytime and night time at thirty spots in Japan, taking into account various kinds of subsoil, and show the following relation (Equation 1):

$$\left[Amplitude(nightime)\right] = 0.3 \times \left[Amplitude(daytime)\right]^{1/2}$$

Equation 1

On the other hand, Haubrich and Akamatsu investigated the low frequency contain of noise (Haubrich, et al. 1963, Akamatsu, et al. 1992). According to the works of Longuet-Higgins, and later Friedrich et al. (Longuet-Higgins 1950, Friedrich, Krüger and Klinge 1998), there is a good correlation between microseisms amplitude (below 1 Hz) and swell height. The predominant period of microseisms is equal to half the natural period of swell height.

As already mentioned, improvements on arrays techniques since the fifties have been favourable to investigate the nature of noise. In 1968, to investigate the direction of noise propagation, Toksöz used the frequency – wave number technique (F-K) on LASA (Large Aperture Seismic Array) data in Montana (United States) (Toksöz, et al. 1968). At low frequencies (0.2 to 0.6 Hz), he determined two distinct noise sources both linked with ocean activity (Pacific Ocean and Labrador Sea).
With the same array analysis (F-K, maximum likelihood (Capon, Greenfield and Kolker 1967, Capon 1969)), Horike observed in Osaka (Japan) a distribution of microseisms sources along the Osaka bay at low frequency (0.68 to 0.8 Hz). These noise sources are due to water waves striking the coast. At higher frequency (1.4 to 1.7 Hz), microtremors sources are caused by traffic in Osaka city.
The work of Satoh (Satoh, Kawase and Shin'ichi 2001) provides another illustration of that point. In the Sendai basin (Japan), during one night, they conduct arrays measurements with 3-components seismometers (frequency band pass 0.025 to 70 Hz). Figure 1-3, displays noise propagation directions estimated by F-K analysis on vertical components (F-K, maximum likelihood (Capon, Greenfield and Kolker 1967, Capon 1969)). For frequencies close to 2 Hz, propagation directions are concentrated in the northwest direction, and in lower frequencies they are relatively scattered in the southeast quadrant. Hence, microseisms are coming from coastal line of the Pacific Ocean, and microtremors from Sendai City. Once more, these results support the idea that sources of long-period noise (microseisms) are mainly oceanic waves, and sources of short-period noise (microseisms) are due to human activities such as traffic or machineries vibrations.

According to these results, we can conclude that two distinct noise origins exist: natural and anthropic. Depending on this origin (natural or anthropic) the comportment of noise is different (in time and spectral domains). Microtremors amplitudes have daily and weekly variations, while natural noise exhibits amplitude variations linked with natural phenomena. We then can establish a boundary between microseisms and microtremors. The frequency limit is around 1 Hz.
We can synthesize all the results about the origin of noise and draw the following scheme:

- frequency < 0.5 Hz   : due to oceanic and large scale meteorological conditions;
- frequency ~ 1 Hz   : due to wind effects and local meteorological conditions;
- frequency > 1 Hz   : due to human activities.

The 1 Hz boundary however, is not a universal limit. According to Seo (Seo 1997) depending on the geology, the limit between microseisms and microtremor can be shifted to lower frequency. In deep soft basin, there could be enough energy to excite the microtremor at frequencies lower than 1 Hz. This phenomenon is shown Figure 1-4, displaying two noise recording at Mexico (one horizontal component); the first one is located on sedimentary site (SCT) and the second one on rock site (UNAM). Differences in the comportment of noise amplitude can be noticed in the time domain: there are daily variations on sediment site, while the variations on rock site are not correlated with night and day alternations. There is the same phenomenon in spectral domain: daily variations of noise spectral amplitude over all the frequency range on sedimentary site, while the daily variations appear only for frequency upper than 1 Hz on rock site.
In the same paper, Seo shows results from other continuous noise measurements (3 weeks) from Rokko Island (Kobe, Japan). He presents the time variation of spectral amplitude of microtremor for horizontal component in shorter period range 0.2- 0.5 seconds (Figure 1-5 top), and the longer period range 1-3 seconds (Figure 1-5 bottom) with that of sea wave heights at Kobe in the Osaka bay and Sakihama of the Pacific coast. From the upper Figure (short period range) we recognise the microtremor behaviour, i.e. daily and weekly variation of noise. For longer period (1-3 s), we note a slightly daily variation but we don't observe

the weekly variation. In other hand, the daily variation of the swell height on Osaka bay is highlighted on the figure. These observations can't allow us to assert or not the assumption of Seo. Do the geologic basin characteristics explain the contamination of natural noise by microtremor? Does a daily variation of natural noise exist? Until now this question is still open.

4 Nature of noise

The origin of noise is not the only interest of scientists. Earlier in the century, several scientists investigated the composition of noise wavefield in order to define its nature.
We can qualify the first study about noise of historic prelude to contemporary research (since 80's up to now). This formula is not pejorative, its underline the higher confidence in new study thanks to the progress on instrumental quality, computer capacity and improvement on processing.
To define the nature of noise, we propose to determinate the three following ratios:
-    the ratio of body waves to surface waves;
-    the ratio of Love waves to Rayleigh waves;
-    the ratio of fundamental Rayleigh mode to higher modes.

4.1 Ratio of body waves to surface waves

In 1968, Toksöz and Lacoss (Toksöz and Lacoss 1968) performed a F-K analysis with array 3-components data from LASA (Large Aperture Seismic Array), Montana (USA). They use 21 broadband seismometers 3-components. They compared the phase velocity of observed waves thanks to arrays analysis with the theoretical phase velocity computed from the soil model. After Figure 1-6, Toksöz and Lacoss draw the following conclusions about the nature of noise:
-    at 2 Hz the observed phase velocity about 3.5 km/s. Such a value correspond to the theoretical phase velocity of the 1st or 2nd higher mode of Rayleigh waves;
-    at 0.3 Hz they identified two distinct velocities. The 3.5 km/s velocity corresponding to Rayleigh waves, and another equal to 13.5 km/s. This second velocity is attributed to compressional body waves (P waves) since there are the only waves to propagate in soil with this velocity. Hence there is a mix of different waves at this frequency (higher modes of Rayleigh waves and P waves);
-    between 0.4 and 0.6 Hz, only the P waves are detected with a velocity of 13.5 km/s;
-    in the frequency range lower than 0.15 Hz, these authors assume that waves are fundamental Rayleigh waves with no more discussions.

Douze (1964, 1967) performed noise measurements in deep borehole (Douze 1964, 1967). He compared the observed and theoretical ratio of deep noise to surface noise amplitude. Figure 1-7 shows the variation of the observed ratio over period for the Eniwetok Island borehole (1288 m deep, Marshall Islands). We clearly note the decrease of this ratio for periods lower then 2 seconds (F > 5 Hz). This amplitude decrease with depth suggests that these waves are surface waves. In the period range beyond than 2 seconds, the ratio is close to 1 indicates that we have body waves (no decrease of amplitude with depth).
The comparison of observed and theoretical ratio of deep noise to surface noise amplitude over period is shown in Figure 1-7 for 3 distinct periods (0.5, 1 and 2 sec). The deep noise dataset comes from the Apache borehole (2917 meters deep, Oklahoma). Douze concludes that:
-    at 0.5 sec (2 Hz), noise is a mix between P waves and 3rd Rayleigh waves mode
-    at 1 sec (1 Hz), it is still a mix between P waves and 1st Rayleigh waves mode
-    at 2 sec (0.5 Hz), it is difficult to establish clear conclusions. However, with regards to Figure 1-7 it seems to be a mix between P waves and 1st Rayleigh waves mode.

Both studies of Toksöz (1968) and Douze (1964, 1967) constitute historical research for the reasons quoted in introduction. Now, let focus on more recent studies and start with the work of Yamanaka et al. in 1994 (Yamanaka, et al. 1994).
They performed continuous noise measurements (10 minutes over 2 hours) in the northwest part of Kanto plain (Japan). They use two sensors composed by three 1-component seismometer with 2 seconds natural frequency. The sensors are put on different sites: one on a sedimentary site and the other on rock site. Figure

1-8 show the comparison between the spectral ratio of horizontal to vertical noise components and the theoretical curve of fundamental Rayleigh waves mode for the sedimentary site (HMY). We observe a good fit between the H/V ratio and the ellipticity of Rayleigh waves (fundamental mode). This observation supports that microseisms in the frequency range (0.1 to 1 Hz), in this, site are mainly constituted by Rayleigh waves.

During the 80's, Li et al. (1984) and Horike (1985) used the same method to determine the nature of noise. They compared observed phase velocity (obtain with arrays techniques) with theoretical wave velocities in known soil.
At Lajitas (south west of Texas), for the frequency range [1-20 Hz] Li et al. have shown that microtremor is a mix between higher Rayleigh modes and/or P waves (Li, et al. 1984).
Horike investigated noise in lower frequency range at Osaka (Japan) (Horike 1985). He used F-K arrays analysis on eleven recording (1-component, natural frequency 1 Hz). He concluded that:
- between 0.5 and 0.9 Hz, noise is constituted by fundamental Rayleigh waves;
- between 0.9 and 2.98 Hz, he detects fundamental Rayleigh mode mixed with higher modes.

Table 1-2 synthesize author's conclusions about nature of noise. At lower frequency (below 1 Hz), microseisms seems to be mainly constituted by fundamental Rayleigh waves (Li et al., Horike, Yamanaka et al.). However there is no agreement between authors to define nature of noise at higher frequency: this is a mix of P waves and Rayleigh waves (fundamental mode and/or higher modes)?

4.2 Ratio of Rayleigh waves to Love waves

For all studies presented in this section, authors have assumed that noise is mainly constituted of surface waves.

In 1998, Ohmachi and Umezono (Ohmachi, et al. 1998) simulate noise in resolving surface waves equation of propagation in simple model: one layer over a halfspace (equations established by (harkrider 1964)). For soil models and excitation type (number, position and direction of forces) they showed a relation between the H/V ratio and the coherency of horizontal and vertical noise component. According to them, this coherency computation would be a good indication of the Rayleigh to Love ratio. Neitherless their simulation shows a variation in the ratio of Rayleigh waves in noise depending on the excitation type (vertical, transverse or radial force), the observation direction, and the impedance contrast of soil. This ratio varies between 10% and 90% with an average around 30%! It seems to be difficult to establish reliable conclusion of the Rayleigh to Love ratio after these results.

Chouet et al. published a study devoted to volcanic tremor of Stromboli volcano (Italy) (Chouet, et al. 1998). In May 1992 they performed array volcanic tremor measurements (different apertures) with short period seismometers (0.5 sec). They use the spatial auto-correlation method developed by Aki (Aki 1957, 1964) and then computed the spatial auto-correlation coefficients between each signal recording on sensors. To obtain the dispersion curve of Rayleigh and Love waves they inverse the spatial auto-correlation coefficients. The Rayleigh waves dispersion curve is obtained thanks to vertical component of noise seismograph. To determine the Love waves dispersion curve they fix to a constant the energy ratio between the Rayleigh and Love waves. A good fit between their results and data is obtained for a ratio equal to 0.3. In other word, Love waves carry 70% and Rayleigh waves 30% of the surface-wave power.
However the percentage of energy ratio given is for volcanic tremor and not for microtremor and it is not right to consider that volcanic tremor and microtremor should necessary have the same behaviour. That is why in this paper the method used by Chouet et al. is more interesting than the result.

Yamamoto used the same technique than Chouet et al. to estimate the energy ratio between Rayleigh and Love waves (Yamamoto 2000). The array observations in this study were carried out at 3 distinct sites of Morioka city (Japan). The natural frequency of the 3-compononent seismometers is 1 Hz. On the contrary of Chouet et al., he determined the proportion of Rayleigh and Love waves as a function of frequency. He presents the results in the frequency range 3 to 10 Hz, for Nioh site (Figure 1-9). Depending on frequency, 60% to 85% of noise energy is carried out by Love waves (frequency range 3 to 8 Hz). For the two other

sites he observed different ratio, but these values are always higher than 50%. He concludes that for urban sites, in the frequency range 3 to 10 Hz, there is more energy carried out by Love waves than Rayleigh waves in microtremor.

In order to determine theoretical formulas to simulate microtremor H/V ratio, Arai and Tokimatsu need to know the amplitude ratio between Rayleigh to Love waves (Arai, et al. 1998, 2000). They used 3-component data obtained with array measurements performed in Japan at four sites (A: Yumenoshima (Tokyo), B: Rokko Island (Kobe), C: Asahi (Kushiro), D: Kotobuki (Kushiro)). As Yamamoto they determine the energy ratio between Rayleigh to Love waves as a function of the frequency. To evaluate this ratio they conducted F-K "beam forming" analysis of radial and transverse motions, and three-dimensional spatial auto-correlation method (Figure 1-10). For the four sites, in the period range 0.08 to 1 seconds (0.08 to 3 seconds for site B (Rokko Island)), this ratio varies around an average value equal to 0.7 (independently to the method used). Hence for frequencies upper than 1 Hz (anthropic noise) noise is constituted by 70% of Love waves and 30% of Rayleigh waves.

In 1999 Cornou installed an array constituted by thirteen 3-component seismometers (3 Lennartz Le3D-0.05 sec and 10 Guralp CMG40-20s) in Grenoble city (France). Continuous records were performed over four months (February to May 1999) (Cornou 2002, Cornou, et al. 2003, 2003) . Using the MUSIC high resolution array analysis (Schmidt 1981) she investigated low frequency noise (lower than 1 Hz) in the Grenoble basin. She noted that the velocities of waves crossing the arrays are close to theoretical surface waves velocities, and then estimated the energy ratio between Rayleigh and Love waves. The ratio of energy carried by radial and transverse components, over all energy contained in noise give the proportion of Rayleigh and Love waves in noise (Equation 2).

$$E\left(vertical + radial\ component\right) / E\left(total\right) = proportion\ of\ Rayleigh\ waves \qquad \textit{Equation 2}$$

Figure 1-11 presents the results obtained for the different days and hours analysed. For the frequency range 0.2 to 1 Hz Cornou points out a proportion around 60% of Rayleigh waves contained in microseisms.

Table 1-3 synthesises results obtained by all authors about the proportion of Rayleigh and Love waves in noise. Given the very few case studies, it is impossible to deduce general conclusions about this proportion. For more or less the same frequency range (higher than 1 Hz) and the same method (spatial auto-correlation method) the results pointed out by Yamamoto and Arai et al. are in agreement, but lack of precision. For lower frequencies (lower than 1 Hz) it is also difficult to conclude since only one study has been done (Cornou in 2002).
Although the conclusions about the ratio of Rayleigh and Love waves in noise are not conclusive there is a common point in each study: there are based on array analysis. The 3-component array analysis seems to be the best way to determine the proportion of Love waves and Rayleigh waves in noise.

4.3 Ratio of fundamental Rayleigh waves mode to higher modes

Actually, the existence of Rayleigh higher modes in noise has been seldom investigated in literature. Precedent sections highlight the lack of knowledge about nature of noise wavefield (body or surface waves ? Rayleigh or Love waves ?). Unfortunately since we have no definition to these questions it is also difficult to determine the ratio between fundamental and higher modes of Rayleigh waves contained in noise.

Without bringing quantitative answer to this question Tokimatsu shows the possible existence of higher mode of Rayleigh waves in noise (Tokimatsu 1997). He computed noise synthetics resolving the displacement equations of Rayleigh waves in stratified soil, and determined the dispersion curve with array analysis. The excitation is a single point force distributed at the surface of the model. For three different shear waves velocity profiles, he computed Rayleigh waves dispersion curve (circle on Figure 1-13). The stiffness of soil layers increases with depth in case 1, while it varies irregularly with depth in case 2 and 3. In the first case with V_s increasing with depth, computed dispersion curve follows the theoretical dispersion curve of fundamental Rayleigh mode. In the second and third case, by contrast, higher mode or multiple higher modes play a significant role at higher frequencies. In case 2, over 30 Hz, the higher the frequency,

the higher becomes the order of higher mode. In case 3, the fundamental mode dominates except in the frequency range 9 to 16 Hz. Hence depending on the geological characteristics of soil (velocity inversion at depth) higher modes in numerical noise can be excited.

Although Tokimatsu does not give any quantitative answer about the proportion of Rayleigh higher modes in noise, he points out that:

- higher modes of Rayleigh waves can exist in noise;
- soil stratification (shear waves velocity profile) plays an important role in excitation of higher modes.

5 Conclusions

Conclusions drawn by authors concerning the nature of noise show are consistent. Depending on the natural or anthropic origin (i.e. low frequencies microseisms or higher frequencies microtremor), characteristics of noise is different in both spectral and temporal domain. The microseisms spectral amplitudes variations are correlated with natural phenomena and there is an agreement that microseisms are due to oceanic and large scale meteorological conditions. On the opposite, microtremor spectral amplitudes variations present a clear correlation with human activities (daily and weekly variations), so microtremors are linked with human activities such as machineries, cars ... The boundary between these two types of noise (microseisms and microtremors) is close to 1 Hz, but may vary from site to site depending on the soil frequency. More advanced investigations have to be done to define the exact frequency limit between microseisms and microtremor, and determine the possible role played by the soil geological characteristics for noise comportment.

Concerning the nature of noise, this literature overview highlights the lack of knowledge. There is no agreement between authors about the composition of noise wavefield. Through this literature review, we ca not give suitable answers to the three ratios to characterize noise. However this study provides indications as to possible way to investigate noise wavefield:

Deep noise measurements in borehole may to be an appropriate way to estimate the ratio of body waves to surface waves in noise. The comparison between theoretical and observed eigenfunction of surface waves for known sites could be a good way to estimate the proportion of surface waves in noise.

On the other hand, 3-component array measurements can allow characterising which surfaces waves are present in noise. Antenna (or arrays) techniques like SPAC or MUSIC can estimate the proportion of Rayleigh and Love waves in noise.

Besides, this state of art highlights the importance of numerical noise simulations to gain further insight into noise structure, and investigates in-depth the noise wavefield.

Chapitre 2: 1D numerical simulations and nature of noise wavefield

1 Introduction

The purpose of this chapter is to analyze the structure of noise wavefield, and more specifically investigate the proportion of surface waves and body waves in microtremor linked with the H/V ratio peaks frequencies. For computational time consuming consideration (see previous SESAME progress report for more details), we use a method of numerical simulation of urban noise (Hisada's code (Hisada 1994, 1995)) based on the wave number method. We compute noise synthetics for well-known 1D structure (a sedimentary layer overlaying a bedrock), for different source types, source distances, and sources depth. The main goals are (1) to define the noise sources to simulate H/V ratio, (2) to investigate the composition of noise wavefield (body and/or surface waves) at H/V ratio frequencies peak.

2 Description of the model

2.1 Soil model

We consider a simple physical model representative of a soft site. It is composed of one homogeneous layer over a half-space, and is called M2 model thereafter. This model is characterized by his thickness, P-wave velocity, S-wave velocity, mass density, and quality factors for P and S-wave (Table 2-1). The physical characteristics of the M2 model have been chose in order to illustrate the properties of a high impedance contrast (about 6.5) between the sedimentary layer and the bedrock. It has been shown in the literature that the shape of the H/V ratio is at least partially controlled by the polarization curve of fundamental Rayleigh wave (e.g. Lachet and bard, 1994). (Tokimatsu 1997, Konno and Ohmachi 1998, Malischewsky, et al. 2003) show that, in two layered medium, if the impedance contrast between the two layer is higher than 3 or 4, the polarization of Rayleigh waves is purely horizontal at frequency close to the resonance frequency; this means that the peak amplitude ratio of fundamental Rayleigh waves ellipticity becomes infinite. Then, as the impedance contrast is high, in the two layered model considered in this study, the agreement between the fundamental Rayleigh wave ellipticity curve and the fundamental S wave resonance frequency is rather good at the resonance frequency (Figure 2-1). While at the first resonance harmonic frequency, there is a shift between the ellipticity curve of the first higher mode of Rayleigh wave and the S wave resonance.

2.2 Sources – receivers configuration

The noise recorded in urban areas can be considered to be caused by a set of sources randomly distributed with varying amplitude. These sources have different origins: cars, factories, wind, rain, etc. We choose to model the sources by a single body force where the direction, the maximum amplitude, and the time function are random (Moczo, et al. 2002). The body force amplitude is defined in the three directions (X, Y, Z), and the vector's length is normalized at one. As seen previously, the maximum investigated frequency is 15 Hz. A total of 290 receivers located at the surface have been defined to compute noise synthetics. 289 receivers are arranged around a central receiver, the aperture of this global array is around 750 meters, and the minimum distance between each receiver is 16 meters (Figure 2-2).
Three characteristics have been taken into account in the numerical scheme to compute the noise synthetics:

1) the type of source time function: in this study, we consider either a delta-like signal (to simulate transient noise sources such as men steps or cars) or a pseudo-harmonic signal (a harmonic carrier with a Gaussian envelope to simulate continuous noise sources such as machinery in factories);

2) the source depth location: in this study, we consider five depths 2, 14, 22 meters (within the sedimentary layer), and 30, 62 meters (inside the bedrock);

3) the source-receiver distance: here we consider four sets with increasing distances (R1, R2, R3 and B sets). R1 set includes distance's sources lower than 500 meters from receiver array center, R2 set includes distances between 500 and 750 meters, R3 set includes distances between 750 and 1250 meters, and B set includes distances larger than 1250 meters. The R1, R2 and R3 sets have been selected to model local sources (source-receiver distances are between 4 and 50 times the sedimentary layer thickness), while the B set model far sources.

3 Methods used to analyze noise wavefield

3.1 Numerical simulation technique

The code developed by Hisada (Hisada 1994, 1995) generates synthetics seismograms using the wave number method and has been used to modeling noise. This code computes the Green's functions dues to point sources for viscoelastic horizontally stratified media, with near and equal source and receiver depths. The response of the structure is then convolved with a chosen source function (source function spectra is filtered between 0.5 and 15 Hz), and the noise synthetic obtained in each receiver positions is the sum (in time domain) of synthetics seismograms due to all sources contributions. For each calculation, it is necessary to specify some numerical parameters like the time samples number (1024 points), the numerical time sampling rate (0.07 seconds) and the minimum period (0.07 seconds). Thus the final duration of our simulated seismograms is 71.68 seconds, and the maximum computed frequency is 14.28 Hertz. Figure 2-3 presents in time and spectral domain, the three-component noise synthetic computed in the center of the model.

3.2 Computation of the horizontal to vertical spectral ratio

The technique originally proposed by Nogoshi and Igarashi (Nogoshi and Igarashi 1971), and wide-spread after its promotion by Nakamura (Nakamura 1989, 1996) aims at estimating some site characteristics related with the site transfer function, using microtremor measurements. It consists in deriving the ratio between the Fourier spectra of the horizontal and the vertical components of the microtremor recording obtained at the surface. While many scientists only trust the peak frequency of this ratio, interpreted as linked to the Rayleigh wave ellipticity and representative of the fundamental S-wave resonance frequency for sites with large enough impedance contrast, some other claim the H/V ratio provides a satisfactory estimate of the site S-wave transfer function.

In our study, the spectra of three components are calculated on the noise synthetics for 30 seconds long windows, these windows are overlapping by 20% of samples per windows. The resulting spectra are smoothed following Konno and Ohmachi (Konno and Ohmachi 1998), with a parameter b equal to 40. The H/V ratios are calculated, for each window, dividing the quadratic mean of the horizontal spectra by the vertical spectrum. Then the final H/V ratio is obtained by averaging the H/V ratios from all windows.

3.4 Array processing

The frequency-wavenumber based method (*f-k*) is one of the main array techniques used for deriving the phase velocity dispersion curves from ambient vibration array measurements. In this study, we have used the

conventional semblance based frequency-wavenumber method (CVFK) implemented in CAP software developed within the framework of the SESAME project (Task B). The conventional semblance based *f-k* method has been developed by Kvaerna and Ringdahl (1986). Only the vertical component of the noise synthetics is used for deriving the dispersion curve. The CVFK estimates (in sliding window manner and narrow frequency bands around some center frequency) the parameters of propagation (direction and slowness) of the most coherent plane wave arrival. For all presented *f-k* approaches we used here a wavenumber grid layout sampled equidistantly in slowness and azimuth resolution (azimuth and slowness resolution set to 5 degrees and 0.035 s/km, respectively). The geometrical configuration of the array used to determine the dispersion curve is displayed in Figure 2-4 (a). Nineteen receivers selected among the 290 receivers have been chosen to set a spiral shaped array. The aperture of the array is about 200 meters and the minimum distance between closer receivers is 16 meters; then the wavenumber range resolution of the array is between 0.0155 and 0.1963 rad/m, Figure 2-4 (b).

Figure 2-4 (c) displays an example of the visualization of array analysis results. We visualize the histograms obtained from CVFK analysis as normalized velocities histogram distribution (in frequency-velocity plane). We present only frequency-velocity couple which density upper than 0.75 (i.e., density upper than 75% of the maximum density). The theoretical Rayleigh wave dispersion curves for fundamental and first higher mode are plotted for comparison. In addition, aliasing curve (derived from the aperture of the array) within the array configuration is plotted.

The upper limit is defined by the aliasing curve, while the upper limit is arbitrary defined by the resonance frequency (i.e., 2 Hz). The lower limit is defined by the resonance frequency of the structure since there is a filter effect of the sedimentary layer on noise vertical components (Scherbaum, Hinzen and Ohrnberger 2003). Then the relative energy of noise vertical components is smaller for frequencies lower the resonance frequency, than for frequency upper the resonance frequency. And then, the CVFK scheme is not able to estimate correctly the velocity for frequencies lower than the resonance frequency.

4 Parametric study

We will first present the raw results of ours simulations, and then we will propose an interpretation of the relation of noise wavefield and H/V ratio.

4.1 Effects of source type

The first part of this work consists in investigating the influence of source time functions on H/V ratio. Do the H/V ratio peak characteristics (frequency and amplitude) depend on the source time functions characteristics?

We consider two distance sources sets: R2 and B sets, respectively representative of local and far sources. All sources are located at 2 meters depth. For both sets of sources, noise synthetics have been computed on all receiver positions considering different source characteristics. In the first case, all source time functions are delta-like; in the second case we consider a mix between delta-like (50%) and pseudo-monochromatic (50%) source time functions (the proportions of source time function are given according to the total number of sources in both sets); and in the third case all sources have pseudo-monochromatic source time functions. The H/V ratios obtained for local and far sources (the R2 and B sets, respectively) computed with the different sources characteristics are displayed Figure 2-5. In the three cases (delta-like, either pseudo-monochromatic, or a mix of both), H/V ratios computed from the R2 source set show one clear dominant peak. Whatever the source time function, this peak is located at the resonance frequency (2 Hz). The H/V ratio peak amplitude are equal in case of pure delta-like and mixed source time function, whereas this amplitude is a little bit smaller in case of pure pseudo-harmonic source time functions. In case of far sources, the H/V ratios exhibit two clear peaks. Whatever the source time function, the first peak is located at the fundamental resonance frequency (2 Hz), and the second, significantly (2-3 times) smaller than the previous one (in term of peak amplitude), is located at the first higher harmonic frequency. The existence of this second peak, in this case, will be discussed later.

In conclusion, we confirm Lachet and Bard (Lachet and Bard 1994) results, i.e. the H/V ratio is weakly dependent on source time functions: its frequency is clearly independent, while the amplitude is weakly sensitive.

4.2 Effects of source distance

The second step of this study is to investigate the influence of the distance between sources and receivers on H/V ratios. According to previous results, noise synthetics have been computed considering only delta-like source time functions. All sources are located at 2 meters depth. Noise synthetics are computed separately for the four source sets: R1, R2, R3, and B sources. We did perform array analysis on the nineteen receivers (the spiral geometry), and we have computed the average H/V ratios on the same nineteen receivers. H/V ratios and array analysis are displayed on Figure 2-6.

In all cases, H/V ratios exhibit a peak at the fundamental frequency (2 Hz). For the R3 and B sources sets, the H/V ratio peak at this frequency is a little bit shifted, if the impedance contrast between the sedimentary layer and the bedrock is stronger the frequency shift should disappear. Besides, for the R3 and B sources sets, H/V ratios also show another peak located at the first harmonic of the S-wave resonance frequency, i.e. 6 Hz (a small peak for the R3 sources set and a more significant peak for the B sources set). H/V ratios for R2 and R3 sets also show a third (small) peak located at 4 Hz. This point will be discussed later.

In all cases (R1, R2, R3 and B sources sets), at the frequency corresponding to the main H/V ratio peak (2 Hz), the array analysis show a good fit between the dispersion curve derived from the vertical component and the theoretical dispersion curve of the fundamental Rayleigh wave mode. Concerning the second H/V ratio peak at 6 Hz for the R3 and B sources sets, array analysis show that the noise wavefield is mainly composed of non-dispersive waves. These observations may be summarized in follow:

1) for noise due to local surface sources in one layer model, H/V ratios exhibit one peak located at the resonance frequency. At this frequency, fundamental mode surface waves dominate the wavefield;

2) for noise due to far surface sources in a one layer model, H/V ratios exhibit two peaks: the first peak is located at the resonance frequency (fundamental surface waves dominate the wavefield at this frequency); the second one is located at the first harmonic of the resonance (non-dispersive waves dominate the wavefield at this frequency).

4.3 Effects of source depth

In this part, we focus on the influence of source depth on the H/V ratio. We have selected the local and far sources sets (respectively, the sum of the R1, R2 and R3 sources sets, and the B sources set), and all sources are modeled by a delta-like time function. We consider four sets of sources located respectively at 2, 14, 22, 30 and 62 meters depth. The three first sets (2, 14 and 22 meters deep) are located inside the sediment layer, and the latest is located below the layer. Figure 2-7 shows the H/V ratios computed for all cases (left panel) on the nineteen receivers (spiral configuration). In any case, H/V ratios exhibit a peak at the fundamental frequency (2 Hz). H/V ratios also show a second peak located at the first harmonic resonance frequency (6 Hz) when the noise computation includes far sources (whatever their depth) or deep local sources (sources located below the sedimentary layer). Each time the 6 Hz peak occurs on H/V ratios, array analysis, performed on the nineteen receivers, show that non-dispersive waves dominate the wavefield at this frequency (Figure 2-7, right panel). Therefore, depending on the sources location and sources depth, the origin of the 2 Hz H/V peak seems to be different. In case of local sources located inside the sedimentary layer, the computed dispersion curve agrees with the theoretical dispersion curve of the fundamental Rayleigh wave mode. For far surface sources (inside the layer), the agreement is not as good as in the previous case, nevertheless at the resonance frequency, array analysis show that a part of the computed dispersion curve fit the theoretical dispersion curve of the fundamental mode of Rayleigh wave, while there exist also non-dispersive waves with velocity equal to the bedrock S-wave velocity. For sources located below the sedimentary layer (for both far and local sources) array analysis show that the wavefield is composed only by non-dispersive waves whatever the frequency.

We can synthesize these observations and emit the following working hypothesis:

1) for noise due to local sources located inside the layer: H/V ratios exhibit one strong peak located at the resonance frequency. At this frequency, the fundamental surface waves strongly dominate the wavefield;

2) for noise due to far sources located inside the layer, H/V ratios exhibit two peaks, one of which is located at the resonance frequency. At this frequency, the fundamental mode of surface waves is present in the wavefield. The second peak is located at the first harmonic of the resonance: at this frequency, non-dispersive waves (body waves) strongly dominate the wavefield. This second peak is due to S-wave resonance;

3) for noise due to deep sources (below the layer): H/V ratios exhibit two peaks: one is located at the resonance frequency, and the second at the first harmonic of the resonance. Non-dispersive waves (body waves in case of local sources, and head waves in case of far sources) dominate the wavefield whatever the frequency. H/V peak ratio is not due surface waves.

5 Interpretation and nature of noise wavefield

In order to validate the hypothesis expressed in part IV, "extreme" models (M3 and M4) have been built. These models are based on the M2 model (same thickness, same body wave velocities, same density), the only difference between models M3 and M4 is the quality factor value (Table 2-2). In the M3 model, there is no attenuation in the upper layer (quality factors are equal to 1000), and there a strong attenuation in the half-space (quality factors are equal to 10). On contrary, in the M4 model, there is a strong attenuation in the upper layer (quality factors are equal to 10) and no attenuation in the half-space (quality factors are equal to 1000). Far sources (modeled with delta-like time functions), located at 2 meters depth for both models (M3 and M4), are considered in these tests.

Due to these attenuations properties, we expect the following wavefield characteristics:

1) in case of sources located at 2 meters depth, there is no attenuation of surface waves in the upper layer of the M3 model. We expect a strong excitation of the fundamental mode of Rayleigh wave; and waves propagating in the lower layer (refracted waves) are strongly attenuated and disappear after a short propagation. Wavefield should be dominated by surface waves;

2) in case of sources located at 2 meters depth, there is no surface waves in the M4 model (since these waves are strongly attenuated in the upper layer), only surface distant head waves (which propagate along the sediment-bedrock interface) should be recorded on receivers (far from sources).

Figure 2-8 presents the M3 H/V ratio and array analysis performed on noise synthetics (recorded by the nineteen receivers, sources located at 2 meter depth) and on M4 model (sources located at 2 meters depth). As expected, H/V ratio exhibits only one peak located at the resonance frequency for the M3 model with sources located at 2 meters depth. According to the array analysis, this peak is due to the fundamental mode of surface waves. There is no H/V peak at 6 Hz in this "extreme" model (whatever the source-receiver distance), and there is no energy on FK map at this frequency. Since there is a strong attenuation in the half-space (no wave coming from the bottom), the head waves can not propagate in the M3 model. This means that the H/V ratio peak observed at 6 Hz on the M2 model (with the same sources – receivers configuration), is probably due to such waves. We then conclude that the H/V ratio peak at 6 Hz on the M2 model, in case of far sources located at 2 meters depth, is due to resonating head waves.

M4 model H/V ratios exhibit two peaks at the resonance and at the first harmonic of the resonance. According to the array analysis, non-dispersive waves dominate the wavefield at these frequencies. Since there is a strong attenuation in the upper layer, surface waves can't propagate in the sediment, then H/V ratio peaks are due to body waves propagating in the lower layer and coming from the bottom at the receiver location (head waves). We conclude that H/V ratio peaks, in this case, are due to resonating head waves. These waves can exist in our model since the distance source is larger than the S waves critical distance (the critical distance is about 10 meters, this small distance is due to the high impedance ratio of our model).

We can synthesize these results and do links with H/V experimental condition on the field:

1) if sources are below the sedimentary layer, H/V ratio peaks are due to S waves resonance;

2) if sources are inside the sedimentary layer and far away, H/V ratio shows two peaks. One is due to fundamental surface waves and resonating head waves; the second one is due to head waves;

3) if sources are inside the sedimentary layer, H/V ratio shows one peak due to horizontal ellipticity of fundamental surface waves.

Of course, it is not reliable to do such distinctions of distance sources on the field: when a field microtremor measurement is performed, different distance sources are acting in the same time. For this reason it is more suitable to talk about the relative contributions of near and far sources. Figure 2-9 shows the relative spectral amplitude of noise synthetics computed with different sources (the R1, R2, R3 and B source sets). Since R1 sources and receivers are very close, noise spectral amplitudes have strong amplitude compare to the other source sets. Nevertheless, the main point of this figure is the low level of the noise spectral amplitude computed with far sources (B source set) compared to local sources (sum of the R1, R2 and R3 source sets). Figure 2-10 exhibits the "control" of the resulting H/V curves and F-K map by the local sources. Figure 2-10 shows H/V ratio and array analysis for noise synthetics computed when the contribution of all surface sources are considered (the sum of local and far sources, i.e. the sum of the R1, R2, R3 and B sources sets). This simulation is close to field measurements (noise sources located at various distances), and confirm that in most of cases, observed H/V ratios in field conditions show only one peak (Bard 1998). (Cotton, et al. 1998, Cara, Di Giulio and Rovelli 2003)

As it has been noted previously, H/V ratio computed for the R2 and R3 source sets exhibit a small peak at 4 Hz. At this time we have not consistent arguments to draw clear conclusions about this phenomenon. Nevertheless, we assume that this H/V ratio peak at 4 Hz is not due to identify waves propagating in the structure (i.e., neither body waves nor surface waves). Considering the M2 model, and M3 and M4 "extreme" models (table 2-1 and 2-2), the B sources set (located at 2 meter deep), we compute noise synthetics for receivers distributed along the x axis (in line configuration). Figure 2-11 displays the corresponding H/V ratio amplitudes according to the source-receiver distance. The H/V ratio peak at 4 Hz appears only for the M2 model, this means that this 4 Hz peak is not due to propagating surface waves (no H/V ratio peak at 4 Hz for the M3 model), and is not due to propagating body waves (no H/V ratio peak at 4 Hz for the M4 model). Then we assume that this H/V ratio peak is due attenuation effects of surface waves.

6 Conclusions

We have simulated noise ambient seismic noise for a simple 1D structure (one layer over a half space) in order to in order to thoroughly test the H/V technique for well-controlled conditions and investigate the composition of noise wavefield at the H/V peak frequency. We have performed a parametric study of the effects of the source distribution (time function, spatial location (in 3D plane)) on H/V ratio shapes. The first conclusion outlined by this study is the independence of the H/V ratio regarding the source time functions. We show that the H/V frequency peak is clearly independent on source time functions, while the peak amplitude is weakly sensitive.
We can synthesize the effects of spatial location of sources on H/V ratio shaping, and highlighted links with field experiment:
1) if sources are below the sedimentary layer, H/V ratio peaks are due to S waves resonance;
2) if sources are inside the sedimentary layer and far away, H/V ratio shows two peaks. One is due to fundamental surface waves and resonating head waves; the second one is due to head waves;
3) if sources are close and inside the sedimentary layer, H/V ratio shows one peak due to horizontal ellipticity of fundamental surface waves.

The main result outlined by this study is the control of the H/V shape by local sources. Even if we show that in some case (far and/or deep sources), H/V ratio can exhibit more than one peak, the relative contribution of these sources on the noise wavefield are small. Then we conclude that field noise wavefield at the fundamental resonance frequency is mainly composed by surface wave (Rayleigh and/or Love waves) (in one layer over a half space). This interpretation is in agreement with previous studies which show that surface waves mainly composed field noise wavefield (Horike 1985, Arai and Tokimatsu 1998).

To enhance these conclusions it would be necessary to perform similar parametric study on more realistic structure such as multiple gradient layers and 3D structures (valley). Moreover, to go head in the

investigation of the nature of noise wavefield it would be also interesting to use 3-components array techniques such as SPAC method. The 3-component SPAC method should allow us to determine the relative proportion of Rayleigh and Love waves in noise wavefield.

Acknowledgements

References:

Abeki N., R. S. Punongbayan, D. C. Garcia, I. C. Narag, B. C. Bautista, M. L. P. Bautista, E. L. Banganan, R. A. Tabanlar, D. S. Soneja, K. Masaki, N. Maeda and K. Watanabe, 1996. Site response evaluation of metro Manila using microtremor observation. *Proceedings of the 11th World Conference on Earthquake Engineering.* Acapulco, Mexico.

Abeki N., K. Seo, I. Matsuda, T. Enomoto, D. Watanabe, M. Schmitz, R. Herbert and A. Sanchez, 1998. Microtremor observation in Caracas City, Venezuela. *Proceeding of the Second International Symposium on he Effects of Surface Geology on Seismic Motion.* Yokohama, Japan. **2** 619-624.

Akamatsu J., M. Fujita and K. Nishimura, 1992. Vibrational characteristics of microseisms and their applicability to microzoning. *J. Phys. Earth,* **40**, 137-150.

Aki K., 1957. Space and time spectra of stationary stochastic waves, with special reference to microtremors. *Bull. Earthquake. Res. Inst. Tokyo,* **35**, 415-457.

Aki K., 1964. A note on the use of microseisms in determining the shallow structures of the earth's crust. *Geophysics,* **30**, 665-666.

Al Yuncha Z. and F. Luzon, 2000. On the horizontal-to-vertical spectral ratio in sedimentary basins. *Bulletin of the Seismological Society of America,* **90-4**, 1101-1106.

Alfaro A., F. Gutierrez, T. Sugagna, S. Figueras, X. Goula and L. Pujades, 1997. Measurements of microtremors in Barcelona: A tool for seismic microzonation. *Proceedings of IAMG'97.* Barcelona, Spain.

Alfaro A., L. Pujades, X. Goula, T. Susagna, B. M. Navarro, F. J. Sanchez and J. A. Canas, 2001. Preliminary map of soil's predominant periods in Barcelona using microtremors. *Pure and Applied Geophysics,* **158-12**, 2499-2511.

Ansal A., R. Iyisan and H. Güllü, 2001. Microtremor measurements for the microzonation of Dinar. *Pure and Applied Geophysics,* **158-12**, 2525-2541.

Ansary M. A., F. Yamazaki, M. Fuse and T. Katayama, 1995. Use of microtremors for the estimation of ground vibration characteristics. *Third international conferences on recent advances in geotechnical earthquake engineering and soil dynamics.* St. Louis, Missouri. **2**.

Arai H. and K. Tokimatsu, 1998. Evaluation of local site effects based on microtremor H/V spectra. *Proceeding of the Second International Symposium on he Effects of Surface Geology on Seismic Motion.* Yokohama, Japan. **2** 673-680.

Arai H. and K. Tokimatsu, 2000. Effects of Rayleigh and Love waves on microtremor H/V spectra. *Proceedings of the 12th World Conference on Earthquake Engineering.* Auckland, New Zealand. #2232.

Arai H., K. Tokimatsu and A. Abe, 1996. Comparison of local amplifications estimated from microtremor F-K spectrum analysis with earthquake records. *Proceedings of the 11th World Conference on Earthquake Engineering.* Acapulco, Mexico. #1486.

Asten M. W., 1978. Geological control of the three-component spectra of rayleigh-wave microseisms. *Bulletin of the Seismological Society of America,* **68-6**, 1623-1636.

Asten M. W. and J. D. Henstridge, 1984. Arrays estimators and the use of microseisms for reconnaissance of sedimentary basins. *Geophysics,* **49-11**, 1828-1837.

Bache T. C., P. Marshall and J. B. Young, 1986. High-frequency seismic noise characteristics at the four United Kingdom-type arrays. *Bulletin of the Seismological Society of America,* **76-3**, 601-616.

Banerji S. K., 1924. Microseisms associated with the incidence of the south-west monsoon. *Nature,* **114-2868**, 576.

Banerji S. K., 1925. Microseisms and the Indian monsoon. *Nature,* **116-2928**, 866.

Bard P.-Y., 1998. Microtremor measurements: A tool for site effect estimation ? *Proceeding of the Second International Symposium on he Effects of Surface Geology on Seismic Motion.* Yokohama, Japan. **3** 1251-1279.

Bettig B., P.-Y. Bard, F. Scherbaum, J. Riepl, F. Cotton, C. Cornou and D. Hatzfeld, 2001. Analysis of dense array noise measurements using the modified spatial auto-correlation method (SPAC). Application to the Grenoble area. *Bollettino Di Geofisica Teorica ed Applicata,* **42-3-4**, 281-304.

Bindi D., S. Parolai, M. Enotarpi, D. Spallarossa, P. Augliera and M. Cattaneo, 2001. Microtremor H/V spectral ratio in two sediment-filled valleys in western Liguria (Italy). *Bollettino Di Geofisica Teorica ed Applicata,* **42-3-4**, 305-315.

Bour M., D. Fouissac, P. Dominique and C. Martin, 1998. On the use of microtremor recordings in seismic microzonation. *Soil Dynamics and Earthquake Engineering,* **17**, 465-474.

Capon J., 1969. High-resolution frequency-wavenumber spectrum analysis. *IEEE.* **57** 1408-1419.

Capon J., R. J. Greenfield and R. J. Kolker, 1967. Multidimensional maximun-likehood processing of a large-aperture seismic array. *IEEE.* **55** 192-211.

Cara F., G. Di Giulio and A. Rovelli, 2003. A study on seismic noise variations at Colfiorito, central Italy: implications for the use of H/V spectral ratios. *Geophysical Research Letters,* **30-18**.

Chouet B., G. De Luca, G. Milana, P. Dawson, M. Martini and R. Scarpa, 1998. Shallow velocity of Stromboli volcano, Italy, derived from small-aperture array measurements of Strombolian tremor. *Bulletin of the Seismological Society of America,* **88-3**, 653-666.

Cornou C., 2002. Traitement d'antenne et imagerie sismique dans l'agglomération grenobloise (Alpes françaises): implications pour les effets de site (In french). Thèse de doctorat, *Université Joseph Fourier,* 260 pp.

Cornou C., P.-Y. Bard and M. Dietrich, 2003. Contribution of dense array analysis to identification and quantification of basin-edge induced waves. part I: Methodology. *Bulletin of the Seismological Society of America,* **93-6**, 2604-2623.

Cornou C., P.-Y. Bard and M. Dietrich, 2003. Contribution of dense array analysis to identification and quantification of basin-edge induced waves. part II: Application to Grenoble basin (french Alps). *Bulletin of the Seismological Society of America,* **93-6**, 2624-2648.

Cotton F. and P. Volant, 1998. Observed and simulated noise at Garner Valley downhole array: A test of the possibilities and limitations of Nakamra's technique. *Proceeding of the Second International Symposium on he Effects of Surface Geology on Seismic Motion.* Yokohama, Japan. **2** 625-633.

Delgado J., P. Alfaro, J. Galindo-Zaldivar, A. Jabaloy, A. C. Lopez Garrido and C. Sanz De Galdeano, 2002. Structure of the Padul-Nigüelas basin (S Spain) from H/V ratios of ambient noise: Application of the method to study peat and coarse sediments. *Pure and Applied Geophysics,* **159**, 2733-2749.

Delgado J., C. Lopez Casado, J. Giner, A. Estevez, A. Cuenca and S. Molina, 2000. Microtremors as a geophysical exploration tool: Applications and limitations. *Pure and Applied Geophysics,* **157**, 1445-1462.

Douze E. J., 1964. Rayleigh waves in short-period seismic noise. *Bulletin of the Seismological Society of America,* **54-4**, 1197-1212.

Douze E. J., 1967. Short-period seismic noise. *Bulletin of the Seismological Society of America,* **57-1**, 55-81.

Duval A.-M., P.-Y. Bard, B. Lebrun, C. Lacave-Lachet, J. Riepl and D. Hatzfeld, 2001. H/V technique for site response analysis. Synthesis of data from various surveys. *Bollettino Di Geofisica Teorica ed Applicata,* **42-3-4**, 267-280.

Duval A.-M., J.-P. Méneroud, S. Vidal and A. Singer, 1998. Relation between curves obtained from microtremor and site effects observed after Caracas 1967 earthquake. *Proceedings of the 11th European Conference on Earthquake Engineering.* Paris, France.

Duval A.-M., S. Vidal, J.-P. Méneroud, A. Singer, F. De Santis, C. Ramos, G. Romero, R. Rodriguez, A. Pernia, N. Reyes and C. Griman, 2001. Caracas, Venezuela, site effect determination with microtremor. *Pure and Applied Geophysics,* **158-12**, 2513-2523.

Fäh D., 1997. Microzonation of the city of Basel. *Journal of Seismology,* **1-1**, 87-102.

Field E. H., A. C. Clement, K. H. Jacob, V. Aharonian, S. E. Hough, P. A. Friberg, T. O. Babaian, S. S. Karapetian, S. M. Hovanessian and H. A. Abramian, 1995. Earthquake site-response study in Giumri (formely Leninakan), Armenia, using ambient noise observations. *Bulletin of the Seismological Society of America,* **85-1**, 349-353.

Flores Estrella H. and J. Aguirre Gonzalez, 2003. SPAC: An alternative method to estimate earthquarke site effects in Mexico city. *Geofisica Internacional,* **42-2**, 227-236.

Frantti G., 1963. The nature of high-frequency earth noise spectra. *Geophysics,* **28-4**, 547-562.

Frantti G., D. E. Willis and J. T. Wilson, 1962. The spectrum of seismic noise. *Bulletin of the Seismological Society of America,* **52-1**, 113-121.

Friedrich A., F. Krüger and K. Klinge, 1998. Ocean-generated microseismic noise located with the Gräfenberg array. *Journal of Seismology,* **2**, 47-64.

Gaull B. A., H. Kagami, M. EERI and H. Taniguchi, 1995. The microzonation of Perth, western Australia, using microtremor spectral ratio. *Earthquake Spectra,* **11-2**, 173-191.

Giampiccolo E., S. Gresta, M. Mucciarelli, G. De Guidi and M. Gallipoli, 2001. Information on subsoil geological structure in the city of Catania (eastern Sicily) from microtremor measurements. *Annali di Geophysica,* **44-1**, 1-11.

Guéguen P., J.-L. Chatelain, B. Guillier, H. Yepes and J. Egred, 1998. Site effect and damage distribution in Pujili (Ecuador) after the 28 march 1996 earthquake. *Soil Dynamics and Earthquake Engineering,* **17**, 329-334.

Gupta I. N., 1965. Standing-wave phenomena in short-period seismic noise. *Geophysics,* **30-6**, 1179-1186.

Gutenberg B., 1958. Microseisms. *Advan. Geophys.,* **5**, 53-92.

harkrider D. G., 1964. Surface waves in multilayered elastic media. I. Rayleigh and Love waves from buried sources in a multilayered elastic half-space. *Bulletin of the Seismological Society of America,* **54-2**, 627-679.

Haubrich R. A., W. H. Munk and F. E. Snodgrass, 1963. Comparative spectra of microseisms and swell. *Bulletin of the Seismological Society of America,* **53-1**, 27-37.

Hisada Y., 1994. An efficient method for computing Green's functions for a layered half-space with sources and receivers at close depths. *Bulletin of the Seismological Society of America,* **84-5**, 1456-1472.

Hisada Y., 1995. An efficient method for computing Green's functions for a layered half-space with sources and receivers at close depths (Part 2). *Bulletin of the Seismological Society of America,* **85-4**, 1080-1093.

Horike M., 1985. Inversion of phase velocity of long-period microtremors to the S-wave-velocity structure down to the basement in urbanized areas. *J. Phys. Earth,* **33**, 59-96.

Horike M., 1996. Geophysical exploration using microtremor measurements. *Proceedings of the 11th World Conference on Earthquake Engineering.* Acapulco, Mexico.

Huang H.-C., Y.-T. Yang and H.-C. Chiu, 2002. Site response evaluation using the H/V ratio at the Yan-Liau station in Hualien, Taiwan. *Pure and Applied Geophysics,* **159**, 2715-2731.

Ibs-Von Seht M. and J. Wohlenberg, 1999. Microtremor measurements used to map thickness of soft sediments. *Bulletin of the Seismological Society of America,* **89-1**, 250-259.

Ishida H., T. Nozawa and M. Niwa, 1998. Estimation of deep surface structure based on phase velocities and spectral ratios of long-period microtremors. *Proceeding of the Second International Symposium on he Effects of Surface Geology on Seismic Motion.* Yokohama, Japan. **2** 697-704.

Kagawa T., 1996. Estimation of velocity structures beneath Mexico city using microtremor array data. *Proceedings of the 11th World Conference on Earthquake Engineering.* Acapulco, Mexico.

Kanai K. and T. Tanaka, 1961. On microtremors. VIII. *Bulletin of the Earthquake Research Institute,* **39**, 97-114.

Kanno T., K. Kudo, M. Takahashi, T. Sasatani, S. Ling and H. Okada, 2000. Spatial evaluation of site effects in Ashigara valley based on S-wave velocity structures determined by array observations of microtremors. *Proceedings of the 12th World Conference on Earthquake Engineering.* Auckland, New Zealand.

Kvaerna T. and F. Ringdahl, 1986. Stability of various f-k estimation techniques. *Semiannual technical summary, 1 October-31 March, NORSAR Scientific Report*, Kjeller, Norway. **29-40.**

Konno K., 1996. Amplification factors estimated from spectral ratio between horizontal and vertical components of microtremor. *Proceedings of the 11th World Conference on Earthquake Engineering.* Acapulco, Mexico.

Konno K. and T. Ohmachi, 1998. Ground-motion characteristics estimated from spectral ratio between horizontal and vertical components of microtremor. *Bulletin of the Seismological Society of America,* **88-1**, 228-241.

Kudo K., 1995. Practical estimates of site response. State-of-art report. *Proceedings of the fifth Internationnal Conference on Seismic Zonation.* Nice, France.

Kudo K., T. Kanno, T. Sasatani, N. Morikawa, P. Apostolidis, K. Pitilakis, D. Raptakis, M. Takahashi, S. Ling, H. Nagumo, K. Irikura, S. Higashi and K. Yoshida, 2002. S-wave velocity structure at EURO-SESITES, Volvi, Greece determined by the spatial auto-correlation method applied for array records of microtremors. *Proceedings of the Mini-Symposium on Site Effects Evaluation for Strong Motion Prediction.* Tokyo, Japan.

Lachet C. and P.-Y. Bard, 1994. Numerical and theoretical investigations on the possibilities and limitations of Nakamura's technique. *J. Phys. Earth,* **42**, 377-397.

Lacoss R. T., E. J. Kelly and T. M. Nafi, 1969. Estimation of seismic noise structure using arrays. *Geophysics,* **34-1**, 21-38.

Lebrun B., D. Hatzfeld and P.-Y. Bard, 2001. Site effect study in urban area: Experimental results in Grenoble (France). *Pure and Applied Geophysics,* **158-12**, 2543-2557.

Lermo J. and F. J. Chavez-Garcia, 1993. Site effects evaluation using spectral ratios with only one station. *Bulletin of the Seismological Society of America,* **83-5**, 1574-1594.

Li T. M. C., J. F. Ferguson, E. Herrin and D. H. B., 1984. High-frequency seismic noise at Lajitas, Texas. *Bulletin of the Seismological Society of America,* **74-5**, 2015-2033.

Liu H.-P., D. M. Boore, W. B. Joyner, D. H. Oppenheimer, R. E. Warrick, W. Zhang, J. C. Hamilton and L. T. Brown, 2000. Comparison of phase velocities from array measurements of rayleigh waves associated with microtremor and results calculated from borehole shear-wave velocity profiles. *Bulletin of the Seismological Society of America,* **90-3**, 666-679.

Lombardo G., G. coco, M. Corrao, S. Imposa, R. Azzara, F. Cara and A. Rovelli, 2001. Results of microtremor measurements in the urban area of Catania, Italy. *Bollettino Di Geofisica Teorica ed Applicata,* **42-3-4**, 317-334.

Longuet-Higgins M. S., 1950. A theory of the origin of microseisms. *Philosophical Transactions of the Royal Society of London,* **A243-a**, 1-35.

Luzon F., Z. Al Yuncha, F. J. Sanchez-Sesma and C. Ortiz-Aleman, 2001. A numerical esperiment on the horizontal to vertical spectral ratio in flat sedimentary basins. *Pure and Applied Geophysics,* **158-12**, 2451-2461.

Malagnini L., A. Rovelli, S. E. Hough and L. Seeber, 1993. Site amplification estimates in the Garigliano valley, Central Italy, based on dense arrays measurements of ambient noise. *Bulletin of the Seismological Society of America,* **83-6**, 1744-1755.

Malischewsky P. and F. Scherbaum, 2003. Love's formula and H/V-ratio (ellipticity) of Rayleigh waves. *accepted to WaveMotion*.

Maresca R., M. Castellano, R. De Matteis, G. Saccorotti and P. Vaccariello, 2003. Local site effects in the town of Benevento (Italy) from noise measurements. *Pure and Applied Geophysics,* **160**, 1745-1764.

Maresca R., E. Del Pezzo, M. La Rocca, G. Liguori, G. Milana and C. Sabbarese, 1999. Site response obtained from array techniques applied to the seismic noise: Two examples in Italy. *Journal of Seismology,* **3**, 31-43.

Maruyama Y., F. Yamazaki and T. Hamada, 2000. Microtremor measurements for the estimation of seismic motion along expressway. *Proceedings of the 6th International Conference of Seismic Zonation.* **II** 1361-1366.

Milana G., S. Barba, E. Del Pezzo and E. Zambonelli, 1996. Site response from ambient noise measurements: New perspectives from an array study in central Italy. *Bulletin of the Seismological Society of America,* **86-2**, 320-328.

Miyakoshi K., T. Kagawa and S. Kinoshita, 1998. Estimation of geological structures under the Kobe area using the array recordings of microtremors. *Proceeding of the Second International Symposium on he Effects of Surface Geology on Seismic Motion.* Yokohama, Japan. **2** 691-696.

Miyakoshi K. and H. Okada, 1996. Estimation of the site response in the Kushiro city, Hokkaido, Japan, using microtremors with seismometer arrays. *Proceedings of the 11th World Conference on Earthquake Engineering.* Acapulco, Mexico.

Moczo P. and J. Kristek, 2002. FD code to generate noise synthetics. *SESAME delivrable D02.09*, 31 pp.

Mucciarelli M., 1998. Reliability and applicability of Nakamura's technique using microtremors: An experimental approach. *Journal of Earthquake Engineering,* **2-4**, 1-14.

Nakamura Y., 1989. A method for dynamic characteristics estimation of subsurface using microtremor on the ground surface. *Quaterly Report Railway Tech. Res. Inst.,* **30-1**, 25-30.

Nakamura Y., 1996. Real-time information systems for hazards mitigation. *Proceedings of the 11th World Conference on Earthquake Engineering.* Acapulco, Mexico.

Nakamura Y., 2000. Clear identification of fundamental idea of Nakamura's technique and its applications. *Proceedings of the 12th World Conference on Earthquake Engineering.* Auckland, New Zealand.

Nogoshi M. and T. Igarashi, 1971. On the amplitude characteristics of microtremor (part 2) *(in japanese with english abstract)*. *Journal of Seismological Society of Japan,* **24**, 26-40.

Ogawa Y., K. Shimizu, E. Joji and D. Maejima, 1998. Estimation of peak horizontal ground velocity based on microtremors. *Proceedings of the 11th European Conference on Earthquake Engineering.* Paris, France.

Ohmachi T. and T. Umezono, 1998. Rate of rayleigh waves in microtremors. *Proceeding of the Second International Symposium on he Effects of Surface Geology on Seismic Motion.* Yokohama, Japan. **2** 587-592.

Ohori M., A. Nobata and K. Wakamatsu, 2002. A comparison of ESAC and FK methods of estimating phase velocity using arbitrarily shaped microtremor arrays. *Bulletin of the Seismological Society of America,* **92-6**, 2323-2332.

Parolai S., P. Bormann and C. Milkereit, 2002. New relationships between Vs, thickness of sediments, and resonance frequency calculated by the H/V ratio of seismic noise for the Cologna area (Germany). *Bulletin of the Seismological Society of America,* **92-6**, 2521-2527.

Rodriguez H. S. and S. Midorikawa, 2003. Comparison of spectral ratio techniques for estimation of site effects using microtremor data and earthquake motions recorded at the surface and in boreholes. *Earthquake Engineering and Structural Dynamics,* **32**, 1961-1714.

Satoh T., H. Kawase and M. Shin'ichi, 2001. Estimation of S-wave velocity structures in and around the Sendai Basin, Japan, using arrays records of microtremors. *Bulletin of the Seismological Society of America,* **91-2**, 206-218.

Scherbaum F., K.-G. Hinzen and M. Ohrnberger, 2003. Determination of shallow shear wave velocity profiles in the Cologne/Germany are using ambient vibrations. *Geophysical Journal International,* **152**, 597-612.

Scherbaum F., J. Riepl, B. Bettig, M. Ohrnberger, C. Cornou, F. Cotton and P.-Y. Bard, 1999. Dense array measurements of ambient vibrations in the Grenoble basin to study local site effects. *EOS, Transactions, AGU,* **80-46**, F707.

Seo K., 1997. Comparison of measured microtremors with damage distribution.

Teves-Costa P., L. Matias and P.-Y. Bard, 1996. Seismic behaviour estimation of thin alluvium layers using microtrmor recordings. *Soil Dynamics and Earthquake Engineering,* **15**, 201-209.

Theodulidis N. P. and P.-Y. Bard, 1995. Horizontal to vertical spectral ratio and geological conditions: An analysis of strong motion data from Greece and Taiwan (SMART-1). *Soil Dynamics and Earthquake Engineering,* **14**, 177-197.

Tobita J., N. Fukuwa and M. Nakano, 2000. Estimation of deep and shallow soil structures using H/V spectrum of densely measured microtremor records. *Proceedings of the International Conference on Geotechnical & Geological Engineering.* #0645.

Tokimatsu K., 1997. Geotechnical site characterization using surface waves. *Proceedings of the First International Conference on Earthquake Geotechnical Engineering.* **3** 1333-1368.

Tokimatsu K., H. Arai and Y. Asaka, 1996. Three-dimensional soil profiling in Kobe area using microtremors. *Proceedings of the 11th World Conference on Earthquake Engineering.* Acapulco, Mexico. #1486.

Tokimatsu K., A. Assiociate Member, K. Shinzawa and S. Kuwayama, 1992. Use of short-period microtremors for Vs profiling. *Journal of Geotechnical Engineering,* **118-10**,

Toksöz M. N., 1964. Microseisms and an attempted application to exploration. *Geophysics,* **29-2**, 154-177.

Toksöz M. N. and R. T. Lacoss, 1968. Microseisms: mode structure and sources. *Science,* **159**, 872-873.

Uebayashi H., 2003. Extrapolation of irregular subsurface structures using the horizontal-to-vertical spectral ratio of long-period microtremors. *Bulletin of the Seismological Society of America,* **93-2**, 570-582.

Wakamatsu K. and Y. Yasui, 1996. Possibility of estimation for amplification characteristics of soil deposits based on ratio of horizontal to vertical spectra of microtremors. *Proceedings of the 11th World Conference on Earthquake Engineering.* Acapulco, Mexico.

Yamamoto H., 2000. Estimation of shallow S-wave velocity structures from phase velocities of love- and rayleigh- waves in microtremors. *Proceedings of the 12th World Conference on Earthquake Engineering.* Auckland, New Zealand.

Yamanaka H., M. Dravinski and H. Kagami, 1993. Continuous measurements of microtremors on sediments and basement in Los Angeles, California. *Bulletin of the Seismological Society of America,* **83-5**, 1595-1609.

Yamanaka H., M. Takemura, H. Ishida and M. Niwa, 1994. Characteristics of long-period microtremors and their applicability in exploration of deep sedimentary layers. *Bulletin of the Seismological Society of America,* **84-6**, 1831-1841.
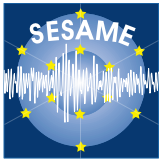
Project Acronym: SESAME

Project Title: Site Effects Assessment Using Ambient Excitations
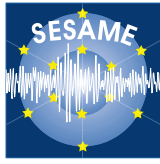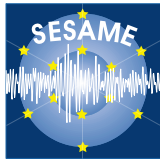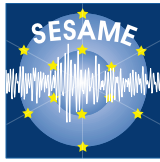**Supported by:** The European Commission – Research General Directorate
Project No: EVG1-CT-2000-00026 SESAME
Report Title: Nature of noise wavefield
Deliverable No: D13.08

	Gutenberg (1958)	Asten (1978-1984)
Waves striking the coast	0.05-0.1 Hz	0.5-1.2 Hz
Moonson / large scale meteorological perturbations	0.1-0.25 Hz	0.16-0.5 Hz
Cyclones over the ocean	0.3-1 Hz	0.5-3 Hz
Local meteorological conditions	1.4-5 Hz	
Volcanic tremor	2-10 Hz	
Urban	1-100 Hz	1.4-30hz

Table 1-1 : Synthesis of noise sources according to frequency after Gutenberg (1958) and Asten (1978, 1984) studies

Project Acronym: SESAME
Project Title: Site Effects Assessment Using Ambient Excitations
Supported by: The European Commission – Research General Directorate
Project No: EVG1-CT-2000-00026 SESAME
Report Title: Nature of noise wavefield
Deliverable No: D13.08

|	0					0.5					1					1.5					2			Hz
Douze 1968						R1/P					R1/P										R3/P			
Toksoz 1964/67	Ro		R+	P/R+		P																		
Li 1984													R+	and / or	P							=>	20hz
Horike 1985					Ro									Ro /	R+								=>	3 hz
Yamanaka 1994			Ro																					

P = Body waves
R*n* = Rayleigh waves
    ***n*=0 : fundamental mode**
    ***n*=1,2 ... : *n* higher mode**
    ***n*=+ : higher modes (no order precision)**

Table 1-2 : Synthesis about nature of noise wavefield obtained from conclusions of different authors (Douze 1968, Toksoz 1964-67, Li 1984, Horike 1985, Yamanaka 1994)
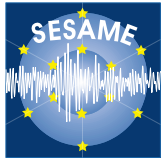
Project Acronym: SESAME

Project Title: Site Effects Assessment Using Ambient Excitations
Supported by: The European Commission – Research General Directorate
Project No: EVG1-CT-2000-00026 SESAME
**Report Title:** Nature of noise wavefield
Deliverable No: D13.08

|	Frequency range	Rayleigh waves (%)	Love waves (%)
Chouet et al. 1998 (volcanic tremor)	*> 2 Hz*	*30 %*	*70 %*
Yamamoto 2000	3 – 10 Hz	< 50 %	> 50 %
Arai et al. 1998	1 – 12 Hz	30 %	70 %
Cornou 2002	< 1 Hz	60 %	40 %

Table 1-3 : Synthesis conclusions about the proportion of Rayleigh and Love waves in noise, after different authors (Chouet et al. 1998 for the volcanic tremor, Yamamoto 2000, Arai et al. 1998, Cornou 2002-03)
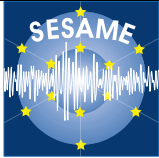
	H (m)	Vp (m/s)	Vs (m/s)	Rho (Kg/m^3)	Qp	Qs
Layer	25	1350	200	1.9	50	25
Half-space	---	2000	1000	2.5	100	50

Table 2-1 : Physical parameters for the sediment site (M2) model (one layer over a half-space).

Project Acronym: SESAME
Project Title: Site Effects Assessment Using Ambient Excitations
Supported by: The European Commission – Research General Directorate
Project No: EVG1-CT-2000-00026 SESAME
Report Title: Final Report of the Nature of Noise Wavefield.
**Deliverable No:** D13.08

	H (m)	Vp (m/s)	Vs (m/s)	Rho (Kg/m^3)	Qp	Qs
M3 model						
Layer	25	1350	200	1.9	1000	1000
Half-space	---	2000	1000	2.5	10	10
M4 model						
Layer	25	1350	200	1.9	10	10
Half-space	---	2000	1000	2.5	1000	1000

Table 2-2 : Physical parameters for the "extreme" models, M3 and M4 (two one layer over a half-space models based on the M2 model).

Project Acronym: SESAME

Project Title: Site Effects Assessment Using Ambient Excitations
Supported by: The European Commission – Research General Directorate
Project No: EVG1-CT-2000-00026 SESAME
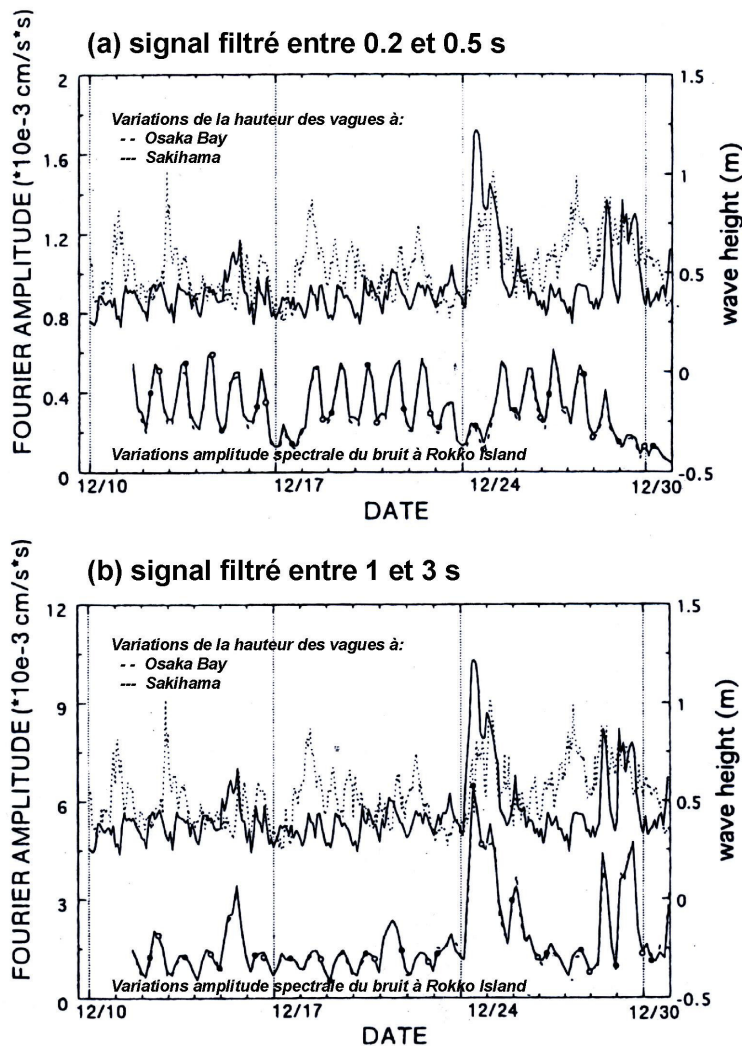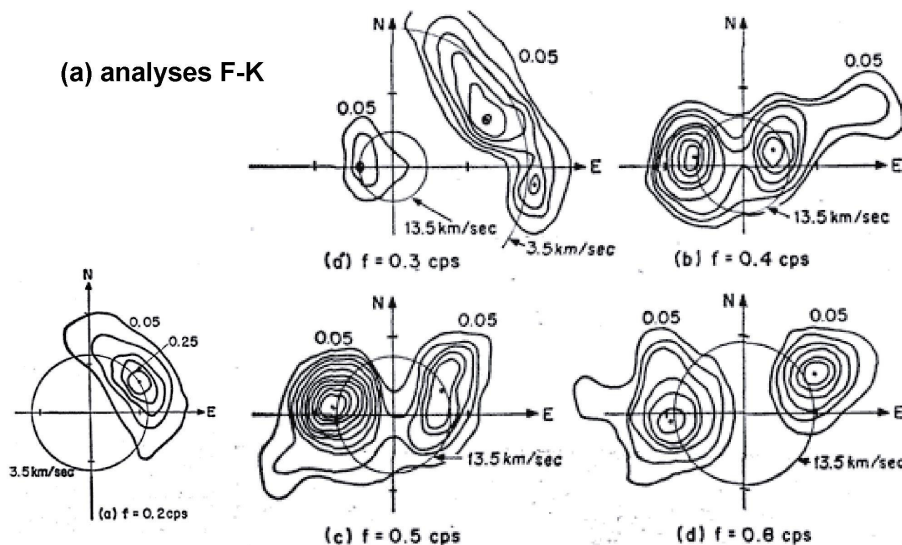**Report Title:** Final Report of the Nature of Noise Wavefield.
Deliverable No: D13.08
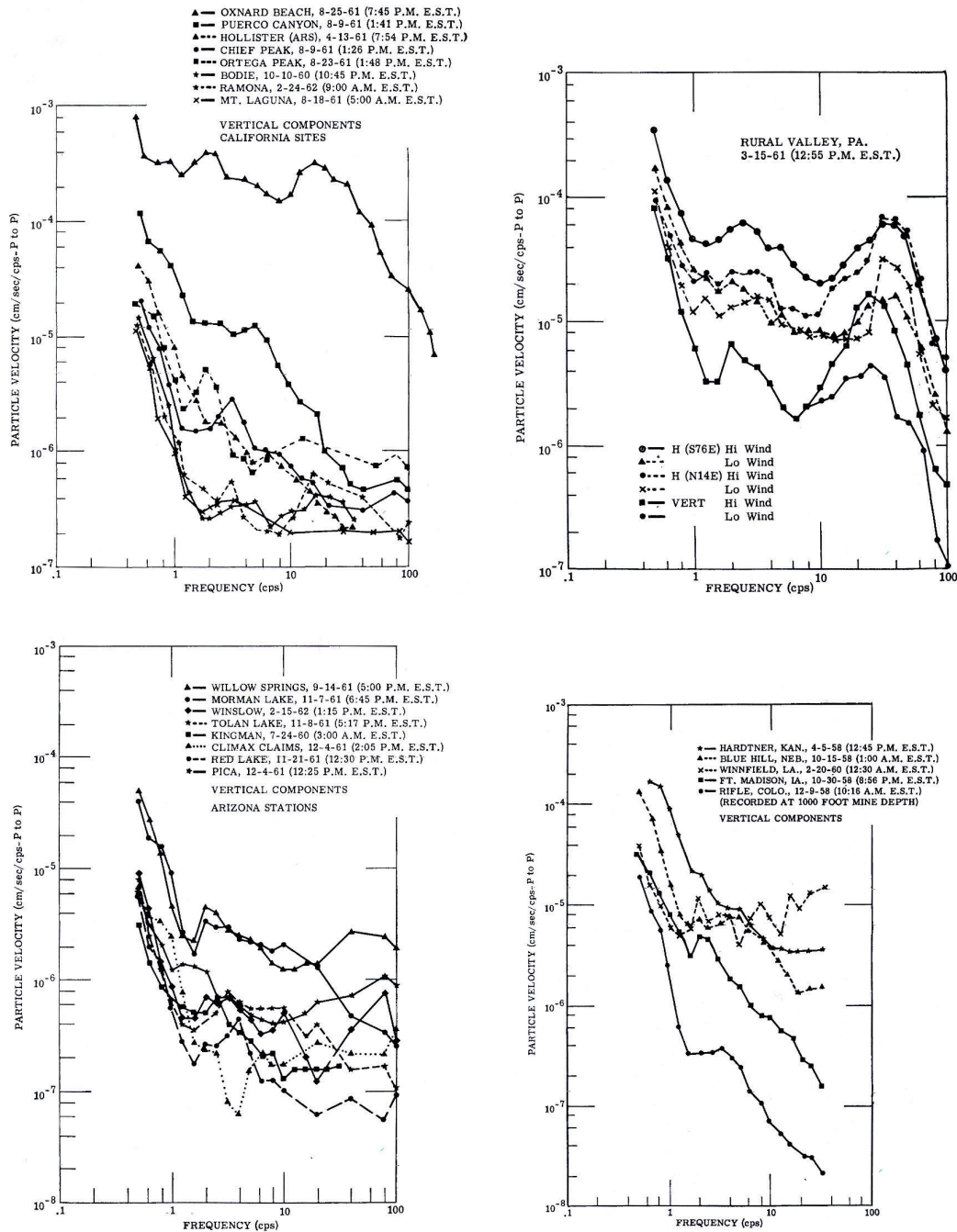
Figure 1-1 : Vertical component of noise particule velocity for 27 locations in United States (after Frantti, 1963)
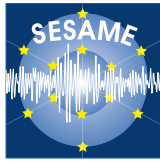
	Project Acronym: SESAME
SESAME	**Project Title:** Site Effects Assessment Using Ambient Excitations **Supported by:** The European Commission – Research General Directorate **Project No:** EVG1-CT-2000-00026 SESAME **Report Title:** Final Report of the Nature of Noise Wavefield. **Deliverable No:** D13.08
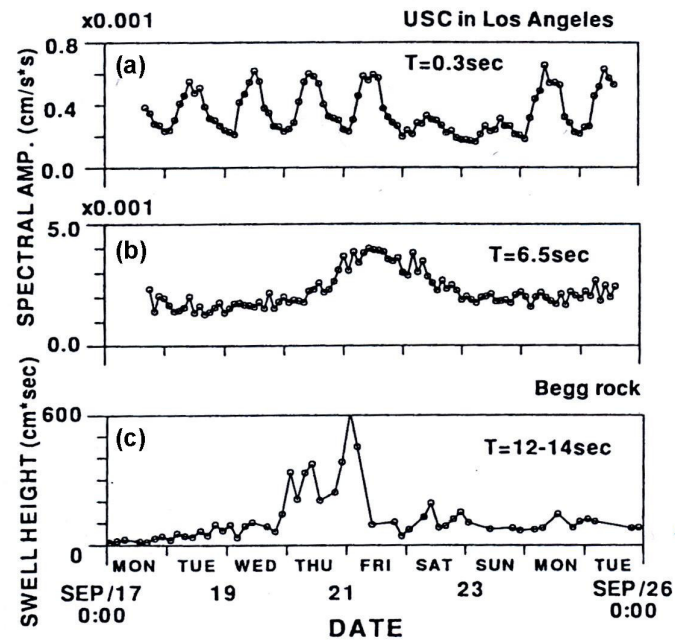
Figure 1-2 : Spectral amplitude variations of noise (Los Angeles) over time (horizontal components) at 0.3 and 6.5 seconds (top). Swell height variations over time recording about a hundred kilometres far from Los Angeles (bottom), after Yamanaka et al. (1993)
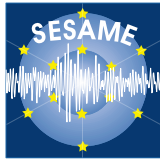
Project Acronym: SESAME
Project Title: Site Effects Assessment Using Ambient Excitations
Supported by: The European Commission – Research General Directorate
Project No: EVG1-CT-2000-00026 SESAME
Report Title: Final Report of the Nature of Noise Wavefield.
**Deliverable No:** D13.08
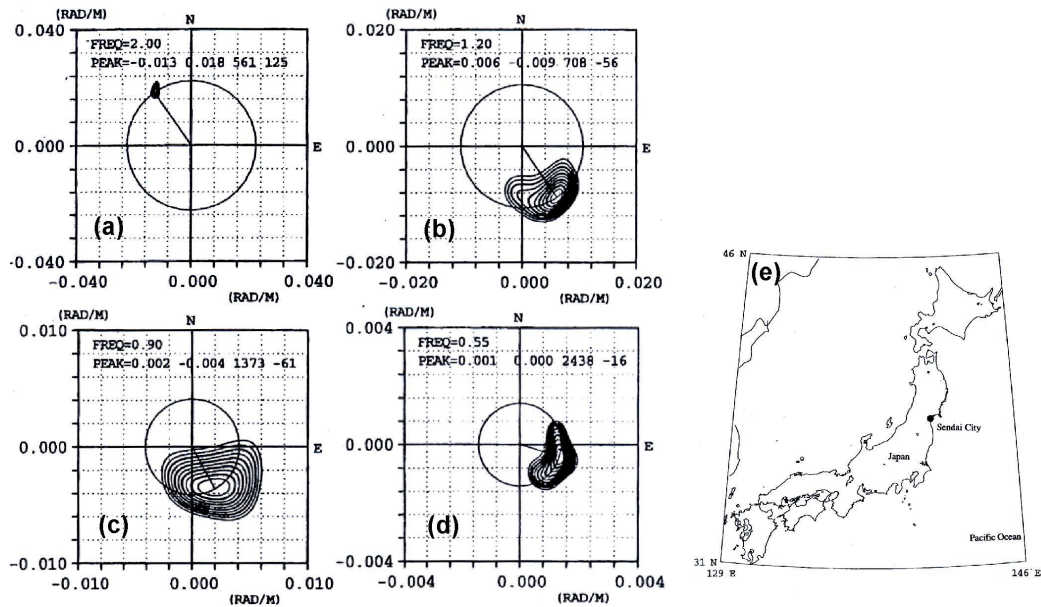
Figure 1-3 : F-K analysis of array measurements in Sendai basin (a-d), localisation of Sendai basin (e), after Satoh et al. (2001)
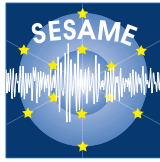
	Project Acronym: SESAME
	Project Title: Site Effects Assessment Using Ambient Excitations
	Supported by: The European Commission – Research General Directorate
	Project No: EVG1-CT-2000-00026 SESAME
	Report Title: Final Report of the Nature of Noise Wavefield.
	Deliverable No: D13.08
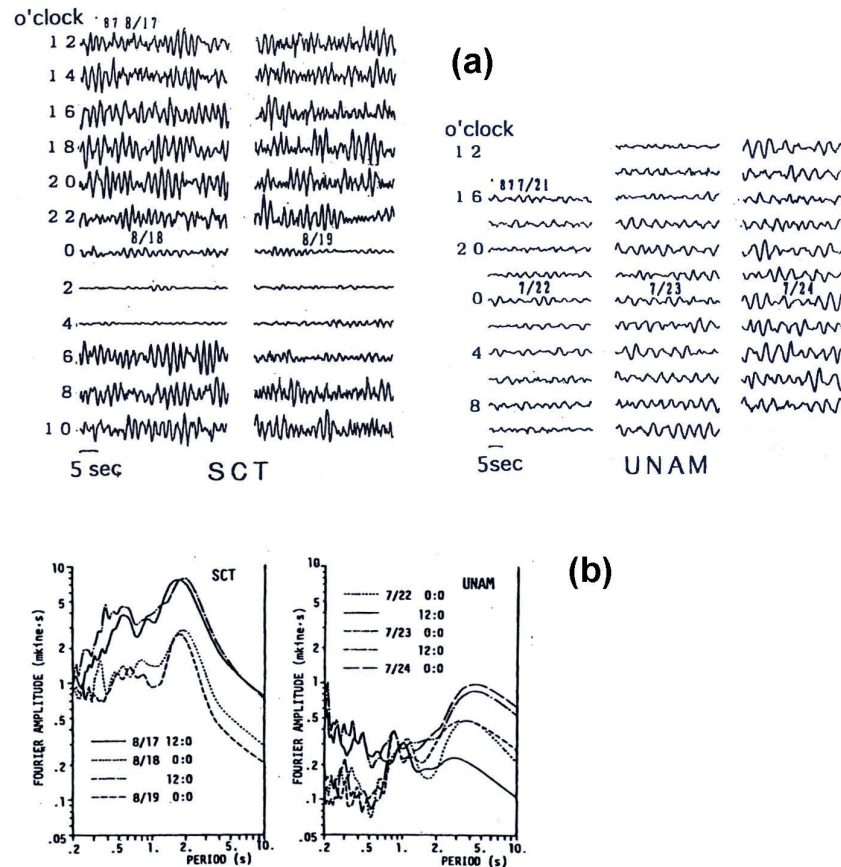
Figure 1-4 : Continuous noise measurements in Mexico. Noise amplitude variations over time for sediment site SCT and rock site UNAM (a). Noise spectral amplitude of SCT and UNAM for different hours (b), after Seo (1996)

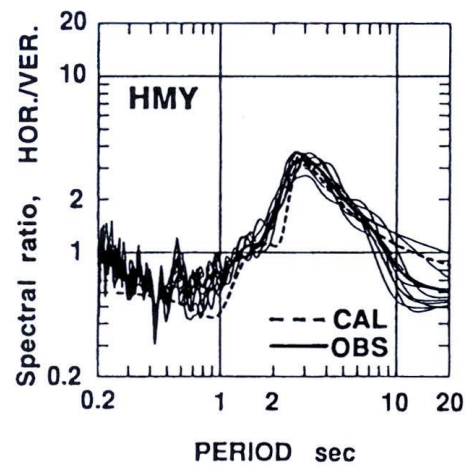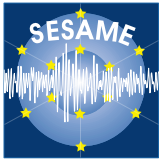|	
![SESAME logo]	**Project Acronym: SESAME** **Project Title:** Site Effects Assessment Using Ambient Excitations **Supported by:** The European Commission – Research General Directorate **Project No:** EVG1-CT-2000-00026 SESAME **Report Title:** Final Report of the Nature of Noise Wavefield. **Deliverable No:** D13.08

Figure 1-5 : Comparison between noise spectral amplitude recording at Rokko Island and swell height variations recording at Osaka bay (plain line) and at Sakihama on pacific coast (dashed line). The results are presented for two period range: 0.2-0.5 sec (a) and 1-3 sec (b), after Seo (1996)

Project Acronym: SESAME
Project Title: Site Effects Assessment Using Ambient Excitations
Supported by: The European Commission – Research General Directorate
Project No: EVG1-CT-2000-00026 SESAME
Report Title: Final Report of the Nature of Noise Wavefield.
**Deliverable No:** D13.08

(a) analyses F-K

(b) courbes de dispersion théorique des ondes de Rayleigh
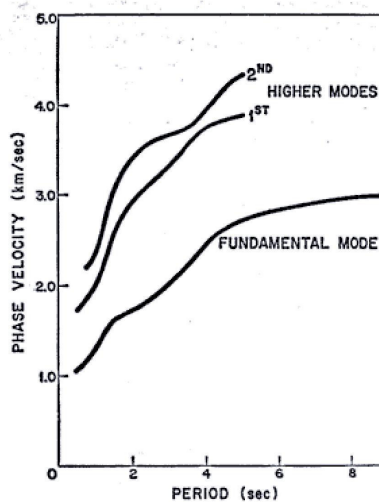
Figure 1-6 : F-K analysis of LASA array at different periods (a), theoretical phase velocity of Rayleigh waves (b), after Toksoz and Lacoss (1968)
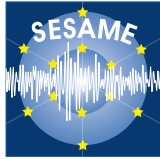
Project Acronym: SESAME
Project Title: Site Effects Assessment Using Ambient Excitations
Supported by: The European Commission – Research General Directorate
Project No: EVG1-CT-2000-00026 SESAME
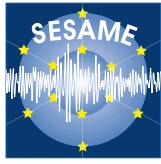**Report Title:** Final Report of the Nature of Noise Wavefield.
**Deliverable No:** D13.08
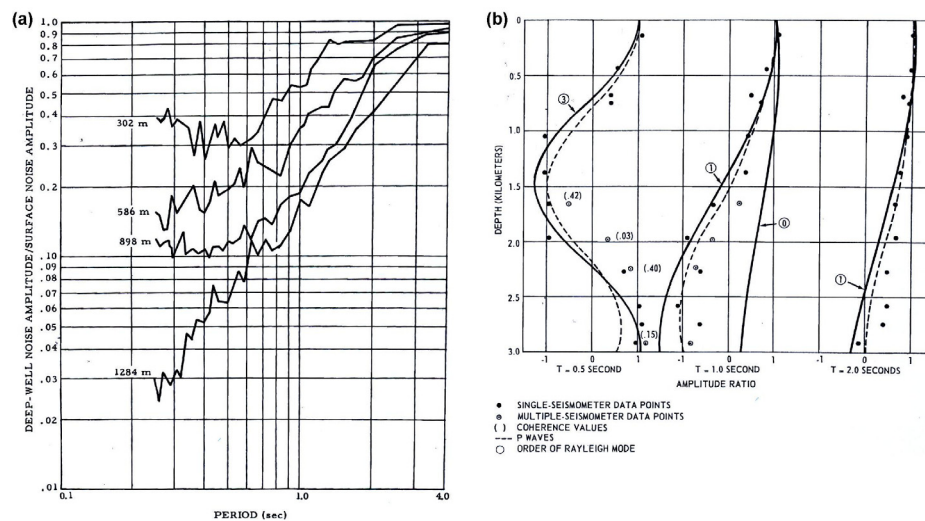
Figure 1-7 : Ratio of deep noise spectral amplitude over surface noise amplitude (vertical component) as a function of period for Eniwetok Island borehole (a) after Douze (1964), and for Apache borehole (b) after Douze (1967). Dots represent observed values, theoretical curve of P waves are in dashed line, and Rayleigh waves in plain line
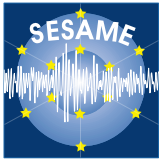
	Project Acronym: SESAME
	Project Title: Site Effects Assessment Using Ambient Excitations
	Supported by: The European Commission – Research General Directorate
	Project No: EVG1-CT-2000-00026 SESAME
	Report Title: Final Report of the Nature of Noise Wavefield.
	Deliverable No: D13.08

Figure 1-8 : Observed spectral ratio H/V (plain line) and theoretical ellipticity curve of fundamental Rayleigh waves mode (dashed line) for HMY site (sediments) at Kanto, after Yamanaka et al. (1994)

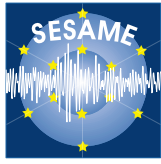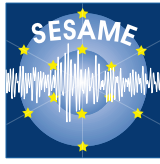|	
![SESAME logo]	**Project Acronym: SESAME** **Project Title:** Site Effects Assessment Using Ambient Excitations **Supported by:** The European Commission – Research General Directorate **Project No:** EVG1-CT-2000-00026 SESAME **Report Title:** Final Report of the Nature of Noise Wavefield. **Deliverable No:** D13.08
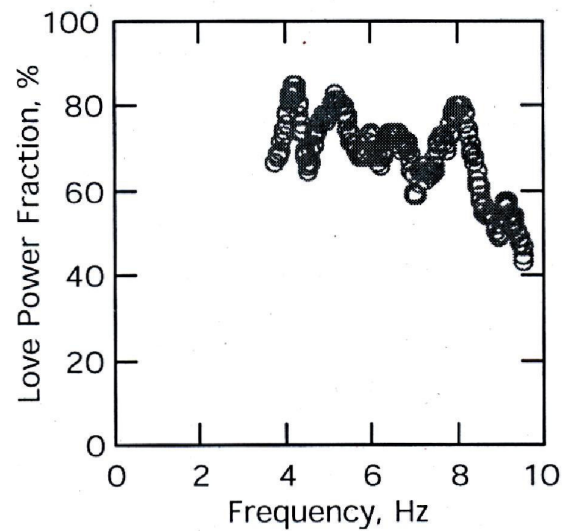
Figure 1-9 : Proportion of Love waves contained in noise in the frequency range 3 to 10 Hz in Nioh site (Morioka, Japan), after Yamamoto (2000)

Project Acronym: SESAME
Project Title: Site Effects Assessment Using Ambient Excitations
Supported by: The European Commission – Research General Directorate
Project No: EVG1-CT-2000-00026 SESAME
Report Title: Final Report of the Nature of Noise Wavefield.
Deliverable No: D13.08
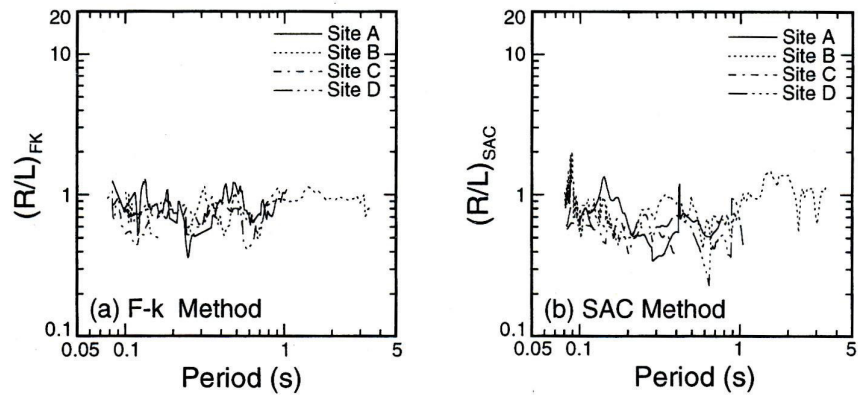
Figure 1-10 : Energy ratio between Rayleigh and Loves waves estimated in four different sites and from 2 array techniques: F-K analysis (a) and spatial auto-correlation method (b), after Arai and Tokimatsu (1998)

Project Acronym: SESAME
Project Title: Site Effects Assessment Using Ambient Excitations
Supported by: The European Commission – Research General Directorate
Project No: EVG1-CT-2000-00026 SESAME
Report Title: Final Report of the Nature of Noise Wavefield.
Deliverable No: D13.08

Julian days	Hours (TU)	Proportion of Rayleigh waves (%)
076	01-02	63+/-7
	15-16	59+/-10
085	01-02	61+/-12
	15-16	63+/-9
090	01-02	65+/-12
	05-06	63+/-15
	15-16	65+/-10
105	01-02	63+/-8
	05-06	65+/-7
	15-16	65+/-7

Figure 1-11 : Figure 11 : Proportion R1 (in %, +/- standard deviation) of Rayleigh waves contained in noise, for different days and hours (high resolution array analysis MUSIC), after Cornou (2002)

Project Acronym: SESAME
Project Title: Site Effects Assessment Using Ambient Excitations
Supported by: The European Commission – Research General Directorate
Project No: EVG1-CT-2000-00026 SESAME
Report Title: Final Report of the Nature of Noise Wavefield.
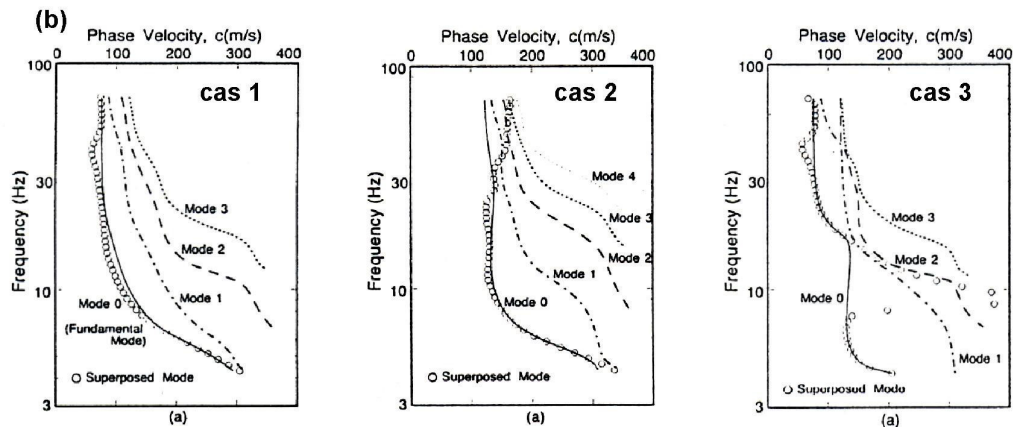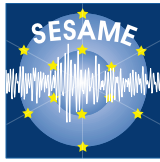**Deliverable No:** D13.08

Figure 1-12 : Velocity profile (a) used by Tokimatsu to compute numerically Rayleigh waves dispersion curves (b). Computed dispersion cures (dots) from noise synthetics are compare with theoretical higher modes dispersion curves of Rayleigh waves, after Tokimatsu (1997)

SESAME	**Project Acronym: SESAME**
	Project Title: Site Effects Assessment Using Ambient Excitations
	Supported by: The European Commission – Research General Directorate
	Project No: EVG1-CT-2000-00026 SESAME
	Report Title: Final Report of the Nature of Noise Wavefield.
	Deliverable No: D13.08
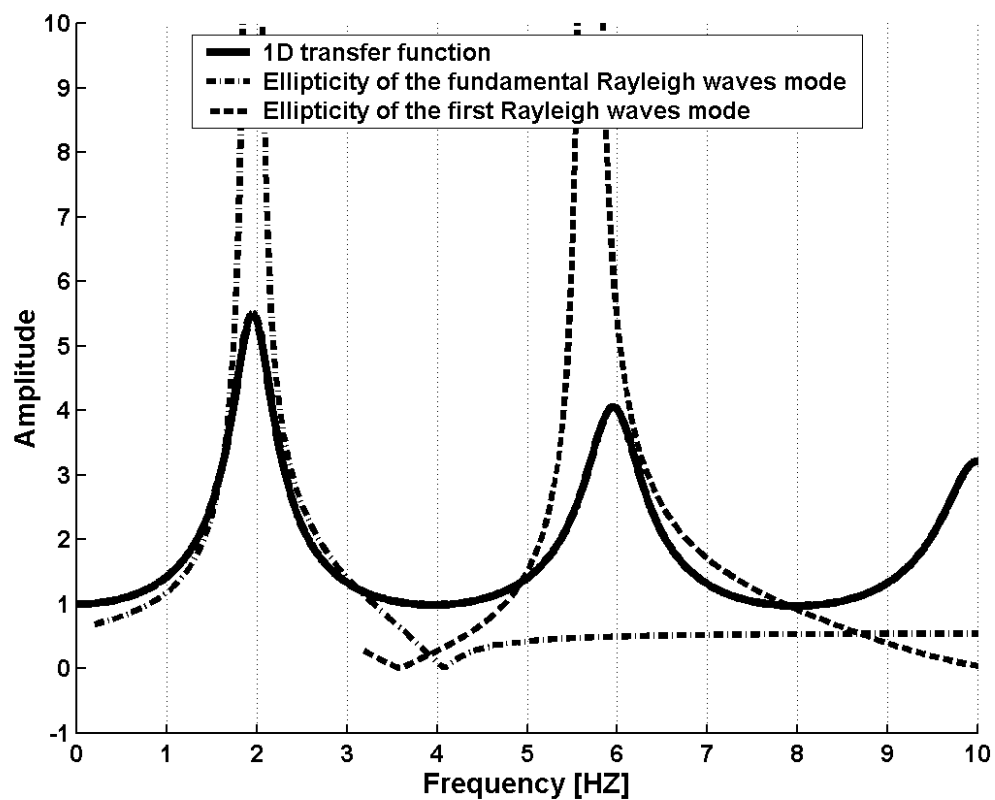
Figure 2-1 : 1D transfer function for vertically incident SH waves (plain line), and the ellipticity of the fundamental mode (dashed line) and the first mode (dashed-dot line) of Rayleigh wave, M2 model.
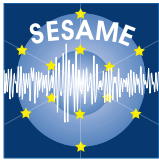
Project Acronym: SESAME

Project Title: Site Effects Assessment Using Ambient Excitations
Supported by: The European Commission – Research General Directorate
Project No: EVG1-CT-2000-00026 SESAME
Report Title: Final Report of the Nature of Noise Wavefield.
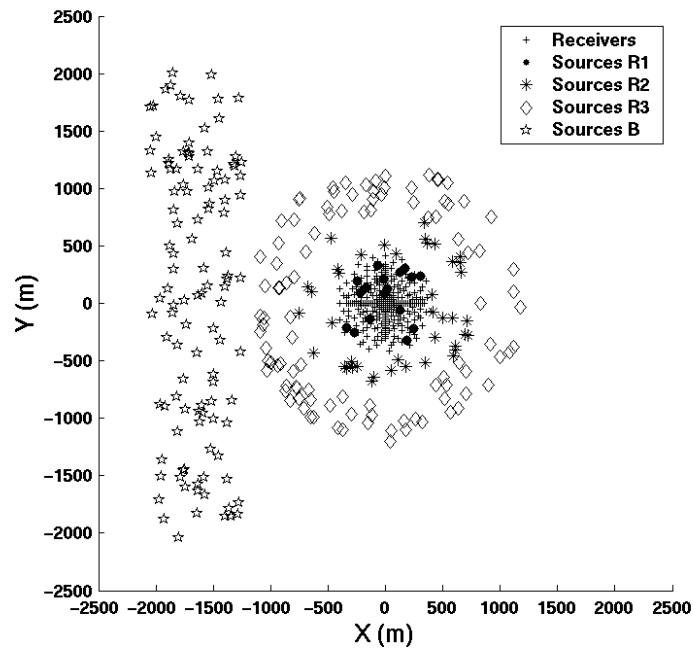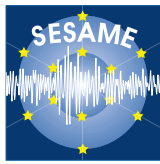**Deliverable No:** D13.08

Figure 2-2 : Spatial distributions of the receivers (cross), and the four sources sets (R1 (dot), R2 (star), R3 (diamond), and B (pentagram)).

Project Acronym: SESAME

Project Title: Site Effects Assessment Using Ambient Excitations
Supported by: The European Commission – Research General Directorate
Project No: EVG1-CT-2000-00026 SESAME
Report Title: Final Report of the Nature of Noise Wavefield.
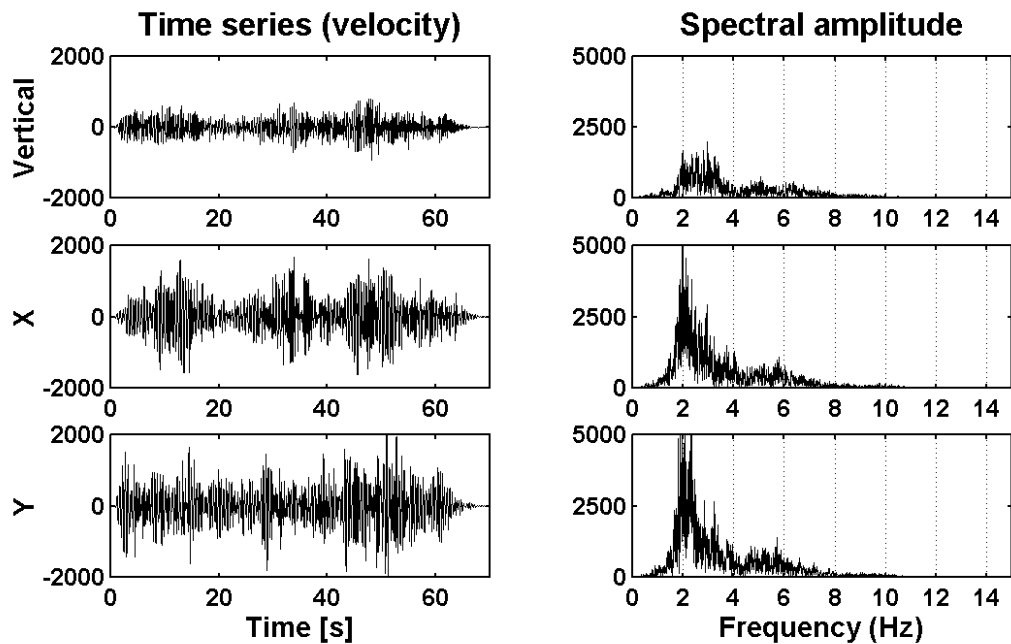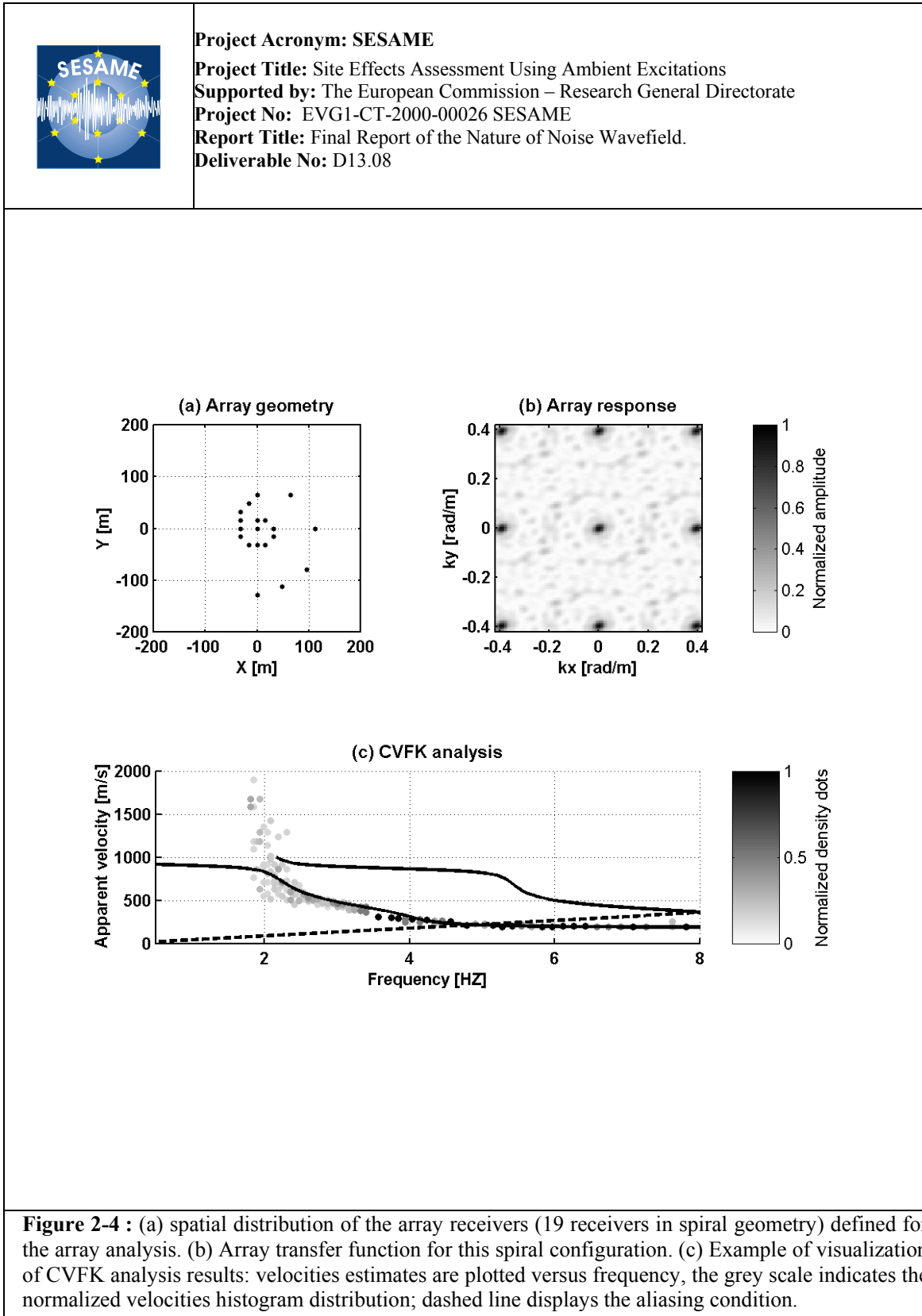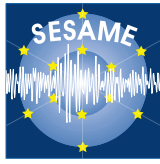**Deliverable No:** D13.08

Figure 2-3 : Synthetic (in the temporal domain (right) and the spectral domain (left)) computed at the surface of the M2 model; the maximum frequency is 14.28 Hertz. The vertical component is represented on the top, north-south component on the middle, and east-west component on the bottom. The time duration of the seismograms is 71.68 seconds.

Project Acronym: SESAME

Project Title: Site Effects Assessment Using Ambient Excitations
Supported by: The European Commission – Research General Directorate
Project No: EVG1-CT-2000-00026 SESAME
Report Title: Final Report of the Nature of Noise Wavefield.
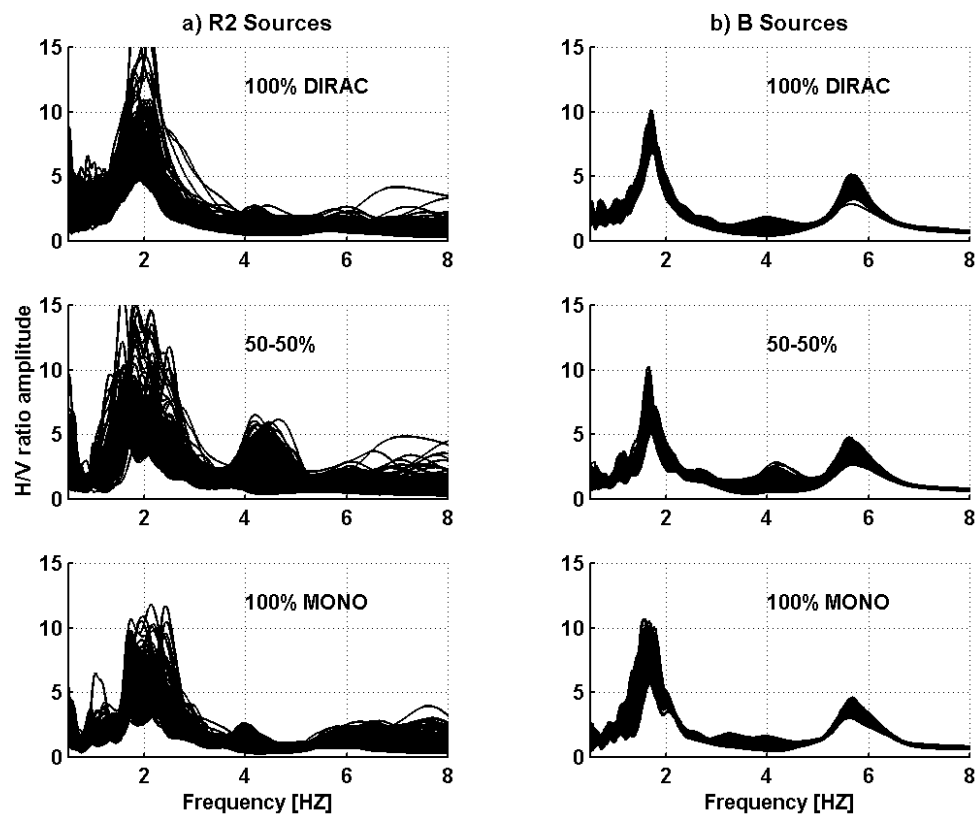**Deliverable No:** D13.08

Figure 2-4 : (a) spatial distribution of the array receivers (19 receivers in spiral geometry) defined for the array analysis. (b) Array transfer function for this spiral configuration. (c) Example of visualization of CVFK analysis results: velocities estimates are plotted versus frequency, the grey scale indicates the normalized velocities histogram distribution; dashed line displays the aliasing condition.

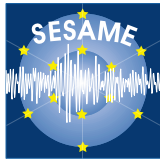|	
SESAME	**Project Acronym: SESAME** **Project Title:** Site Effects Assessment Using Ambient Excitations **Supported by:** The European Commission – Research General Directorate **Project No:** EVG1-CT-2000-00026 SESAME **Report Title:** Final Report of the Nature of Noise Wavefield. **Deliverable No:** D13.08

Figure 2-5 : H/V ratios computed for R2 sources set (a), and for the B sources set (b). (top) 100% delta-like time function; (middle) 50% of delta-like and 50% of pseudo-harmonic time functions (percentage in number of sources); (bottom) 100% of pseudo-harmonic time functions. All sources are located at 2m depth.

Project Acronym: SESAME

Project Title: Site Effects Assessment Using Ambient Excitations
Supported by: The European Commission – Research General Directorate
Project No: EVG1-CT-2000-00026 SESAME
Report Title: Final Report of the Nature of Noise Wavefield.
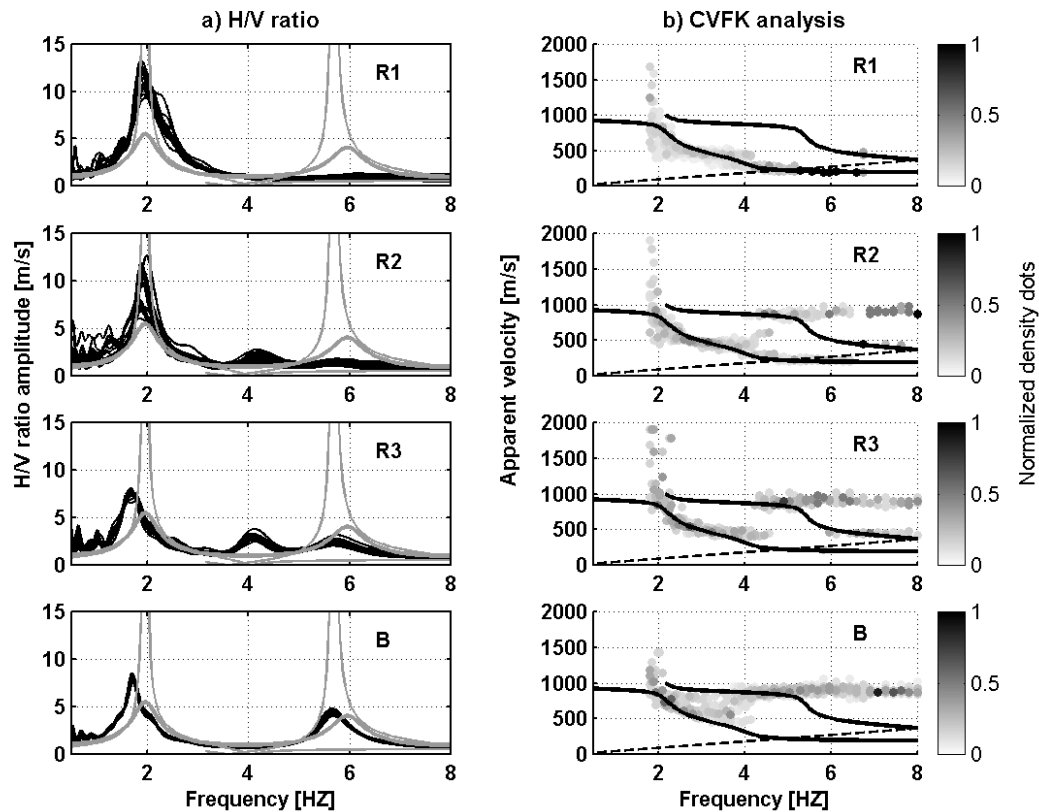**Deliverable No:** D13.08

Figure 2-6 : (a) H/V ratios computed at the array receivers (black curves) for four set of distance sources (R1, R2, R3, and B sources). Thick grey curve displays the 1D transfer function for vertically incident SH waves; thin grey curves display the ellipticity of the fundamental mode and first higher mode of Rayleigh wave, respectively. (b) The corresponding apparent velocities estimated by the conventional *f-k* (CVFK) array method. Grey scale indicates the normalized velocities histogram distribution. Black curves represent the theoretical dispersion curves of the fundamental and the first harmonic of Rayleigh wave (plain lines), and aliasing condition (dashed lines). All sources are delta-like time functions and located at 2m depth.
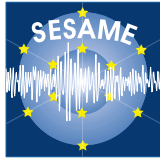
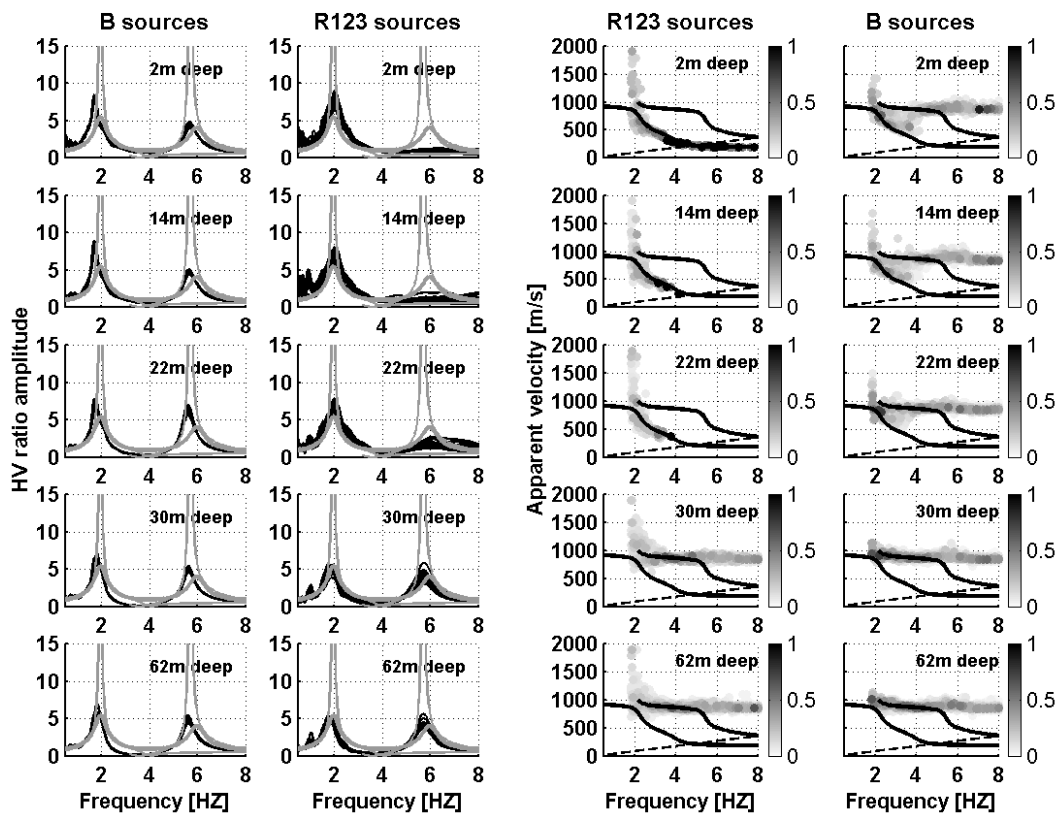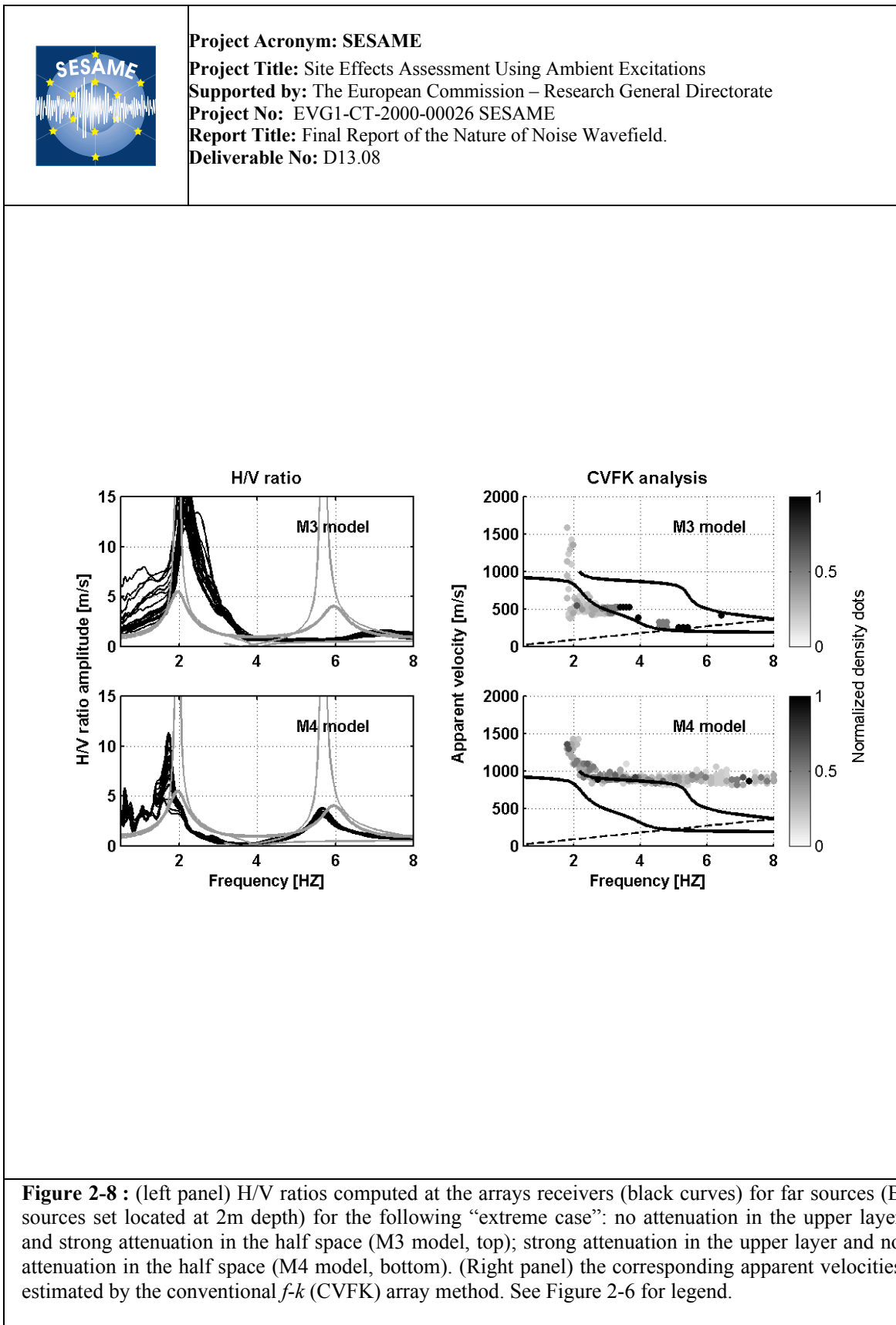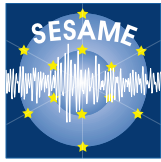|	
	Project Acronym: SESAME **Project Title:** Site Effects Assessment Using Ambient Excitations **Supported by:** The European Commission – Research General Directorate **Project No:** EVG1-CT-2000-00026 SESAME **Report Title:** Final Report of the Nature of Noise Wavefield. **Deliverable No:** D13.08

Figure 2-7 : (left) H/V ratio computed at the array receivers (black curves) for local sources (sum of the R1, R2 and R3 sources set) and far sources (B sources set) located inside the layer (2, 14 and 22 meters depth), and located below the sedimentary layer (30 and 62 meters depth). (right) The corresponding apparent velocities estimated by the conventional *f-k* (CVFK) array method. See Figure 2-6 for legend.

Project Acronym: SESAME

Project Title: Site Effects Assessment Using Ambient Excitations
Supported by: The European Commission – Research General Directorate
Project No: EVG1-CT-2000-00026 SESAME
Report Title: Final Report of the Nature of Noise Wavefield.
Deliverable No: D13.08

Figure 2-8 : (left panel) H/V ratios computed at the arrays receivers (black curves) for far sources (B sources set located at 2m depth) for the following "extreme case": no attenuation in the upper layer and strong attenuation in the half space (M3 model, top); strong attenuation in the upper layer and no attenuation in the half space (M4 model, bottom). (Right panel) the corresponding apparent velocities estimated by the conventional *f-k* (CVFK) array method. See Figure 2-6 for legend.

Project Acronym: SESAME

Project Title: Site Effects Assessment Using Ambient Excitations
Supported by: The European Commission – Research General Directorate
Project No: EVG1-CT-2000-00026 SESAME
Report Title: Final Report of the Nature of Noise Wavefield.
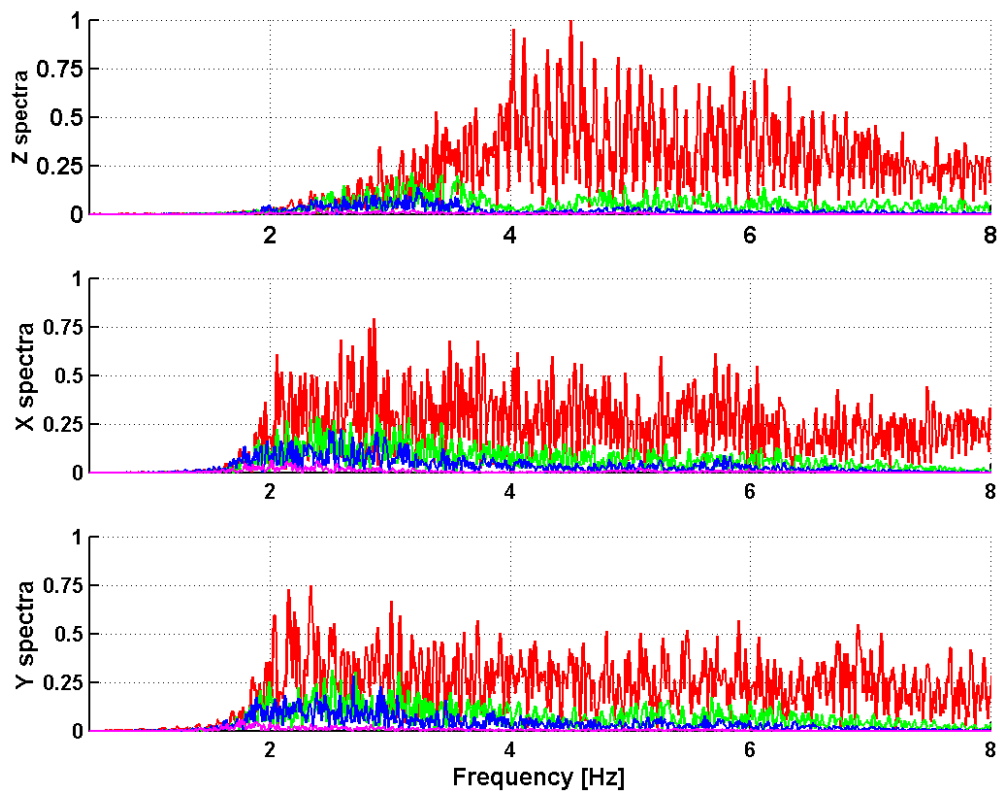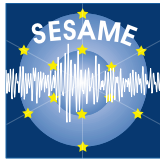**Deliverable No:** D13.08

Figure 2-9 : Relative noise spectra amplitude in the Z (top), X (middle) and Y (bottom) directions. Spectra are computed separately for the four sources sets: R1 (red curves), R2 (green curves), R3 (blue curves) and the B sources (magenta curves) Spectra shown here were computed at the receivers located in the middle of the array.

Project Acronym: SESAME

Project Title: Site Effects Assessment Using Ambient Excitations
Supported by: The European Commission – Research General Directorate
Project No: EVG1-CT-2000-00026 SESAME
Report Title: Final Report of the Nature of Noise Wavefield.
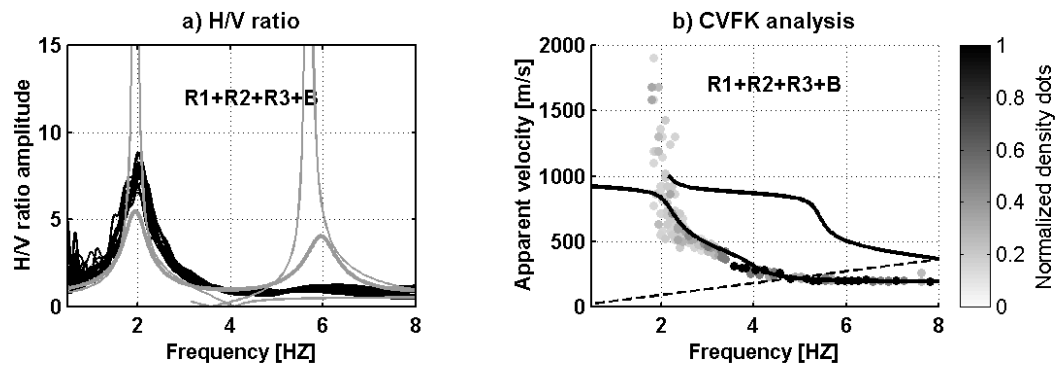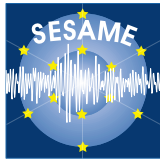**Deliverable No:** D13.08

Figure 2-10 : (a) H/V ratios computed at the array receivers (black curves) for all sources (the sum of the R1, R2, R3, and B sources sets). Sources are located at 2 meters depth. (b) the corresponding apparent velocities estimated by the conventional *f-k* (CVFK) array method. See figure 2-6 for legend.

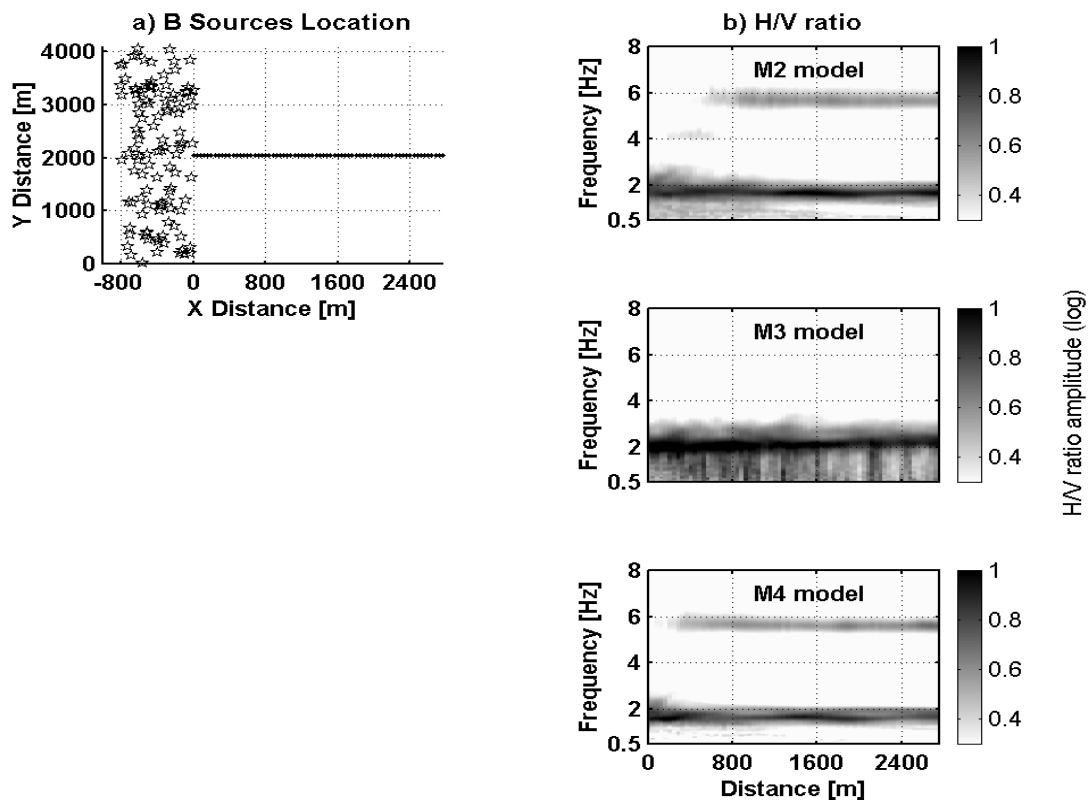|	
![SESAME logo]	**Project Acronym: SESAME** **Project Title:** Site Effects Assessment Using Ambient Excitations **Supported by:** The European Commission – Research General Directorate **Project No:** EVG1-CT-2000-00026 SESAME **Report Title:** Final Report of the Nature of Noise Wavefield. **Deliverable No:** D13.08

Figure 2-11 : (a) spatial distribution of the B sources set and the receivers, receivers are located along a line parallel to x axis. (b) H/V ratios computed at the line receivers for the B sources set for the M2 model (top), the M3 model (middle) and the M4 model (bottom). Sources are located at 2 meters depth. The x axis displays the distance sources-receivers, the y axis displays the frequency, and the color scale displays the logarithm of the H/V ratio amplitude.